Understanding large scale CMB anomalies with the generalized nonminimal derivative coupling during inflation

Yashi Tiwari[,1,*] Nilanjandev Bhaumik[,2,†] and Rajeev Kumar Jain[2,‡]

[1]*Joint Astronomy Programme, Department of Physics, Indian Institute of Science,*
C. V. Raman Road, Bangalore 560012, India
[2]*Department of Physics, Indian Institute of Science,*
C. V. Raman Road, Bangalore 560012, India

We study the observational implications of a class of inflationary models wherein the inflaton is coupled to the Einstein tensor through a generalized nonminimal derivative coupling (GNMDC). In particular, we explore whether these models can generate suitable features in the primordial spectrum of curvature perturbations as a possible explanation for the large-scale anomalies associated with the angular power spectrum of CMB temperature anisotropies. We derive model-independent constraints on the GNMDC function for such a scenario, considering both the scalar and tensor perturbations. We modify CosmoMC to accommodate our GNMDC framework and investigate different classes of inflationary models using a fully consistent numerical approach. We find that the hilltop-quartic model with a specific choice of the GNMDC function provides a considerable improvement over the best-fit reference ΛCDM model with a nearly scale-invariant power spectrum. While the large-scale structure observations should be able to provide independent constraints, future CMB experiments, such as CMB-S4 and CMB-Bharat, are expected to constrain further the parameter space of such beyond canonical single-field inflationary models.

I. INTRODUCTION

Our current understanding of the universe on large scales is remarkably well described by the standard model of cosmology—a relatively simple six-parameter ΛCDM model, supplemented by an inflationary epoch in the very early universe [1–5]. Besides providing an elegant explanation to the numerous shortcomings of the hot big bang theory, an epoch of inflation also provides a causal and efficient mechanism for the origin of primordial density perturbations which source the anisotropies in the cosmic microwave background (CMB) radiation and later act as seeds for the formation of the large scale structures in the universe [6–12]. For these reasons, the inflationary paradigm is now widely considered a crucial part of the concordance model of cosmology. The simplest inflationary models are based on a minimally coupled slowly rolling scalar field, called the *inflaton*, with a slowly varying potential. Such slow-roll inflationary models predict a nearly scale-invariant power spectrum of primordial curvature perturbations with very small non-Gaussianities that are in excellent agreement with the ever-increasing precision measurements of the CMB anisotropies by WMAP and Planck [13–16].

In the CMB measurements at large angular scales, several unexpected features, collectively known as CMB anomalies, have also been observed by COBE, WMAP and Planck [17–19]. Among these anomalies, one of the most notable ones is the low value of the temperature angular power spectrum at the quadrupole moment $\ell = 2$, even below the cosmic variance of the ΛCDM model with a nearly scale-invariant primordial spectrum. Besides, some other outliers (localized features) also exist around $\ell \sim 20$–30. Some localized features also appear at smaller scales, most significantly around $\ell \sim 750$ in the TT and TE spectra, observed by Planck. Although all these features have marginal statistical significance from the Planck data, they have still generated enormous interest in the literature to understand if they could have a primordial origin in the early universe [20,21]. Such features are strongly scale-dependent deviations from an otherwise nearly scale-invariant spectrum. Within the minimal class of canonical single field inflationary models, one of the simplest possibilities to generate these features is to briefly modify the slow roll dynamics of the inflaton, either by introducing a step in the inflaton potential [22–30], allowing an inflection point in the potential [31–34] or imposing kinetic/fast roll initial conditions for the dynamical

*yashitiwari@iisc.ac.in
†nilanjandev@iisc.ac.in
‡rkjain@iisc.ac.in

evolution of the inflaton field [35–39]. All these approaches give rise to localized features in the primordial spectrum, which usually improve the best fit over the concordance model and have been discussed extensively in the literature. Moreover, the possible origin of these primordial features has also been studied in the context of multifield inflationary models [40,41]. In particular, a specific class of two field models that allow a rapid turn in the field space usually produce such features due to transient deviations from the slow roll conditions [42–44].

To extend beyond the minimal setup, an interesting possibility is also to use the scalar-tensor theories such as the Horndeski theory [45]. An interesting aspect of these theories is that despite higher-order terms in the Lagrangian, they yield second-order field equations and, thus, remain free of the Ostrogradsky instability. Within the framework of Horndeski theory, in this paper, we explore specific inflationary scenarios involving coupling of the derivative of the inflaton field to the Einstein tensor with a generalized coupling function, popularly known as the generalized nonminimal derivative coupling (GNMDC) [46–49]. These interactions induce gravitationally enhanced friction, affecting the inflationary dynamics of the scalar field and lead to very interesting phenomenological implications.

The simplest case of GNMDC is called the nonminimal derivative coupling (NMDC), wherein the coupling function is a constant. It has been extensively explored, leading to interesting implications in early universe cosmology [50,51] and black hole physics [52,53]. The drawback of NMDC is due to its constant presence also at the end of inflation and reheating era, which leads to dynamical instability during the reheating stage [54], affects the process of particle production and thus, changes the predictions of the standard reheating scenario [55]. Therefore, the simple NMDC term has been proven to be not so useful for successful inflationary model building. However, in a more general GNMDC setup, all these issues can be cured. The freedom to choose the form of the generalized coupling function makes these classes of GNMDC models phenomenologically attractive. In general, choosing a nonconstant, field-dependent GNMDC function affects the dynamics of the inflaton field, thereby leaving distinguishable imprints in the primordial power spectrum. For instance, the GNMDC term during inflation has been recently studied for forming primordial black holes and induced gravitational waves [56–58]. Including GNMDC coupling or the gravitationally enhanced friction can also make a class of inflationary models consistent with the CMB data, which are otherwise ruled out. Recently, this possibility has also been explored in the context of Higgs inflation assuming slow roll approximations [49].

In this paper, we aim to study whether GNMDC models can help make inflationary scenarios consistent with the latest CMB data and simultaneously explore the prospects of generating localized features in the scalar power spectrum to explain the origin of large-scale features in the angular power spectrum of CMB temperature anisotropies. For simplicity, we only consider the GNMDC function a function of the scalar field ϕ and study three different inflationary models for this purpose. Independent of the choice of the coupling function, we find relevant constraints on this class of GNMDC models by keeping track of the propagation speed for scalar and tensor perturbations. From simple analytical arguments, we show that the generation of nontrivial localized features in the primordial power spectrum to explain the CMB anomalies in these models, together with avoiding any gradient instabilities and unphysical solutions, is inconsistent with subluminal propagation of both scalar and tensor perturbation modes simultaneously. Only if the tensor perturbations are marginally superluminal during the inflationary phase, it opens up the possibility of generating large-scale features of sufficient amplitude in the primordial scalar power spectrum. Staying within these constraints, we find that GNMDC models' efficiency in explaining large-scale CMB anomalies crucially depends on the functional form of the GNMDC function $\theta(\phi)$.

Unlike previous literature, which relies explicitly on the slow roll approximation in GNMDC, we adopt a fully numerical approach and develop a fast parallel computing module to exactly calculate the power spectra of scalar and tensor perturbation in these models, taking into account the transient deviations from the slow roll conditions accurately. With this code, we study the evolution of the background and linear scalar and tensor perturbations accurately. We couple this code to the publicly available cosmological Monte-Carlo code CosmoMC[1] [59] to compare these models with the concordance ΛCDM model and arrive at the best fit parameter constraints. We use two Planck datasets and work with relevant likelihood combinations for our model comparison. For both cases, we show that within the GNMDC setup, characterized by our specific choice of $\theta(\phi)$, we obtain significant improvement in the fit at large scales in the Planck data. As mentioned earlier, the choice of $\theta(\phi)$ is crucial to obtain specific features in the power spectrum. Here, we primarily target the large-scale anomalies around $\ell \sim 20$–30 in the observations of CMB temperature anisotropies by introducing a localized feature in the GNMDC coupling function. Thus, we do not expect much improvement in the fit on relatively smaller scales or in polarization. Nevertheless, we still check the consistency of our model with the small-scale temperature and polarization anisotropy likelihoods for two different datasets to ensure that the introduction of the GNMDC feature does not affect the fit in smaller scales or for polarization likelihood. The freedom to choose $\theta(\phi)$ leaves us with much richer dynamics, and one can further

---

[1]https://cosmologist.info/cosmomc/.

aim to achieve significant improvement on smaller scales as well in CMB. Thus it will be more relevant to study these models with the advent of future observations of CMB polarization, such as from CMB-S4 experiments which should be able to constrain these features better and provide stronger bounds on the parameters space of these models.

This paper is organized as follows. In the following section, we shall briefly discuss the details of the inflationary setup, including the GNMDC term, and derive the equations of motion of the background evolution and the linear scalar and tensor perturbations. In Sec. III, we discuss various issues arising in GNMDC models, such as the gradient instability associated with the scalar perturbations and the superluminal propagation of gravitational waves, and also provide possible resolutions to these problems. In Sec. IV, we discuss our choice of the GNMDC function $\theta(\phi)$ and the various inflationary models that we work with. In Sec. V, we discuss the methodology of our numerical approach that we have developed to compare these models with the data. In Sec. VI, we present our results for the best-fit constraints on various model parameters and the best-fit CMB power spectra. Finally, in Sec. VII, we summarize our results, conclude with a discussion and present some outlook for future work in this direction. In appendix, we present the evolution equations corresponding to the background and perturbations for the GNMDC setup, which we use in our numerical module to compute the power spectra of scalar and tensor perturbations.

Our notations and conventions are as follows. We shall work with natural units such that $\hbar = c = 1$, and the reduced Planck mass $M_{\mathrm{Pl}} = (8\pi G)^{-1/2}$. We shall work in the spatially flat Friedmann-Lemaître-Robertson-Walker (FLRW) universe described by the following line element

$$\mathrm{d}s^2 = -\mathrm{d}t^2 + a^2(t)\mathrm{d}\mathbf{x}^2 = a^2(\tau)(-\mathrm{d}\tau^2 + \mathrm{d}\mathbf{x}^2), \quad (1)$$

where t and τ denote the cosmic time and conformal time, respectively while a represents the scale factor of the 3-dimensional spatial hypersurface. An overdot and over-prime will denote differentiation with respect to t and τ coordinates.

II. GENERALIZED NONMINIMAL DERIVATIVE COUPLING (GNMDC) DURING INFLATION

As mentioned in the Introduction, we explore the implications of a derivative coupling which can be motivated by the well-studied scalar-tensor theory like the Horndeski theory [48,60]. The complete action for the Horndeski theory (or equivalently, for the generalized Galileons), constructed out of the metric tensor and a scalar field, is given as [48]

$$\mathcal{S} = \int d^4x \sqrt{-g} \sum_{i=2}^{5} \mathcal{L}_i, \quad (2)$$

where

$$\mathcal{L}_2 = G_2(\phi, X),$$

$$\mathcal{L}_3 = -G_3(\phi, X)\Box\phi,$$

$$\mathcal{L}_4 = G_4(\phi, X)R + G_{4X}(\phi, X)[(\Box\phi)^2 - (\nabla_\mu\nabla_\nu\phi)^2],$$

$$\mathcal{L}_5 = G_5(\phi, X)G_{\mu\nu}\nabla^\mu\nabla^\nu\phi - \frac{1}{6}G_{5X}[(\Box\phi)^3 - 3\Box\phi(\nabla_\mu\nabla_\nu\phi)^2 + 2(\nabla_\mu\nabla_\nu\phi)^3],$$

where R is the Ricci scalar, G_i are four independent arbitrary functions of ϕ and X, and $G_{iY} = \partial G_i/\partial Y$ with $Y = \{\phi, X\}$ and $X = -\partial_\mu\phi\partial^\mu\phi/2$. For specific choices of the functions G_i, one can reproduce most of the second-order scalar-tensor theory as a specific case. For instance, the nonminimal coupling to gravity can be obtained by setting $G_4 = G_4(\phi)$. Moreover, the Einstein-Hilbert action is already contained in this construction and can be recovered by setting $G_4 = M_{\mathrm{Pl}}^2/2$. For our case, the action comprising of a GNMDC interaction during inflation can be obtained from the Horndeski setup by choosing $G_2 = X - V(\phi)$, $G_3 = 0$, $G_4 = M_{\mathrm{Pl}}^2/2$, $G_5 = G_5(\phi)$, and further doing integration by parts for the term $\mathcal{L}_5$, we arrive at

$$\mathcal{S} = \int d^4x \sqrt{-g} \left[\frac{M_{\mathrm{Pl}}^2}{2}R - \frac{1}{2}(g^{\mu\nu} - \theta(\phi)G^{\mu\nu})\partial_\mu\phi\partial_\nu\phi - V(\phi) \right], \quad (3)$$

where $V(\phi)$ is the potential of the inflaton field and $\theta(\phi) = -2G_{5\phi}$. As mentioned earlier, the case where $\theta(\phi)$ is a constant is referred to as the NMDC. As we shall discuss later, for a given potential, an appropriate choice of the coupling function $\theta(\phi)$ can generate interesting features in the primordial spectrum of curvature perturbations and, therefore, in the CMB angular power spectrum which can possibly explain the observed large scale features in the CMB temperature anisotropies.

For the homogeneous, isotropic, and spatially flat FLRW metric, the background Friedmann equations can be written as [56]

$$3H^2 = \kappa^2 \left[V(\phi) + \frac{1}{2}\dot{\phi}^2(1 + 9\theta(\phi)H^2) \right], \qquad (4)$$

$$-2\dot{H} = \kappa^2[(1 + 3\kappa^2\theta(\phi)H^2 - \kappa^2\theta(\phi)\dot{H})\dot{\phi}^2$$
$$- \kappa^2\theta'(\phi)H\dot{\phi}^3 - 2\kappa^2\theta(\phi)H\dot{\phi}\ddot{\phi}], \qquad (5)$$

where $\theta' = d\theta/d\phi$, $\kappa^2 = 1/M_{\mathrm{Pl}}^2$ and from now on, we set $\kappa^2 = 1$. The Klein-Gordon equation for ϕ can be obtained as

$$\ddot{\phi}(1 + 3\theta(\phi)H^2) + 3H\dot{\phi}(1 + \theta(\phi)(3H^2 + 2\dot{H}))$$
$$+ \frac{3}{2}\theta'(\phi)\dot{\phi}^2H^2 + V'(\phi) = 0, \qquad (6)$$

where $V' = dV/d\phi$. Evidently, all these equations reduce to the case of a single minimally coupled canonical scalar field in the absence of the GNMDC term. Moreover, the presence of the GNMDC term allows for an extra friction term in the equations of motion thereby changing the inflationary dynamics drastically. Using Eq. (4), we find that the velocity of the inflaton field can be obtained as

$$\dot{\phi} = \pm\frac{\sqrt{2[3H^2 - V(\phi)]}}{\sqrt{1 + 9\theta(\phi)H^2}}, \qquad (7)$$

which implies that the real solutions of $\dot{\phi}$ would demand

$$1 + 9\theta(\phi)H^2 > 0, \qquad (8)$$

$$3H^2 > V(\phi). \qquad (9)$$

These conditions together impose a constraint on the GNMDC function $\theta(\phi)$ in terms of the potential of the inflaton field. Therefore, in order to avoid unreal values of the inflaton velocity, we obtain the following condition that we always impose

$$1 + 3\theta(\phi)V(\phi) > 0. \qquad (10)$$

Further, for a given potential $V(\phi)$ and the GNDMC function $\theta(\phi)$, we solve the background equations numerically with the number of e-folds N as the time variable by using appropriate initial conditions on ϕ, $\dot{\phi}$ and H by requiring that
  (i) Inflation lasts for a long enough duration which determines the initial value of the inflaton field i.e. $\phi_i = \phi(N = N_i)$.
  (ii) In order to have negligible deviations from slow roll dynamics at an initial time N_i, we set the initial condition on the Hubble parameter using Eq. (4) as

$$H = \sqrt{\frac{V(\phi)}{3} + \xi}, \qquad 0 < \xi \ll 1. \qquad (11)$$

  (iii) Finally, the initial condition on $\dot{\phi}$ is given by Eq. (7).
  In order to understand the background evolution for a given $V(\phi)$ and $\theta(\phi)$, we have developed a numerical module based on an exact integration of the Friedmann equations which are subject to initial conditions as mentioned above. This is required as we are interested in generating primordial features in the power spectrum of curvature perturbations that may arise due to transient deviation from slow-roll conditions. Since the slow roll approximation is usually not able to correctly capture these features, we shall not discuss the slow roll approximation for the background quantities and the slow roll results for the power spectrum of cosmological perturbations.

We shall now discuss the evolution of linear cosmological perturbations in this scenario and focus only on the scalar and tensor perturbations as vector perturbations usually decay during inflation unless being sourced. Following the standard cosmological perturbation theory at the linear order, the second order action for the scalar curvature perturbations $\mathcal{R}$ can be calculated as [48,60]

$$\mathcal{S}_{\mathcal{R}}^{(2)} = \int dt d^3x a^3 \mathcal{G}_s \left[\dot{\mathcal{R}}^2 - \frac{c_s^2}{a^2}(\partial\mathcal{R})^2 \right], \qquad (12)$$

where c_s is the propagation speed of the scalar modes, given by

$$c_s^2 = \frac{\mathcal{F}_s}{\mathcal{G}_s}, \qquad (13)$$

and $\mathcal{F}_s$ and $\mathcal{G}_s$ are defined as

$$\mathcal{F}_s = \frac{1}{a}\frac{d}{dt}\left(\frac{a}{\Theta}\mathcal{G}_T^2 \right) - \mathcal{F}_T, \qquad (14)$$

$$\mathcal{G}_s = \frac{\Sigma}{\Theta^2}\mathcal{G}_T^2 + 3\mathcal{G}_T, \qquad (15)$$

with

$$\Sigma = X - 3H^2 + 18H^2X\theta(\phi) \qquad (16)$$

$$\Theta = H[1 - 3X\theta(\phi)] \qquad (17)$$

$$\mathcal{F}_T = 1 + X\theta(\phi) \qquad (18)$$

$$\mathcal{G}_T = 1 - X\theta(\phi) \qquad (19)$$

In order to avoid the ghost and gradient instabilities associated with the curvature perturbations, we must

require that $\mathcal{G}_s > 0$ and $c_s^2 > 0$ which, in turn, imposes constraints on the GNMDC coupling function $\theta(\phi)$. In terms of the conformal time $d\tau = dt/a$, the second order action in Eq. (12) can be written as

$$\mathcal{S}_{\mathcal{R}}^{(2)} = \int d\tau d^3 x z_s^2 (\mathcal{R}'^2 - c_s^2(\partial\mathcal{R})^2), \qquad (20)$$

where $z_s = a\sqrt{\mathcal{G}_s}$. Using this action, the Mukhanov-Sasaki equation for the Fourier modes of curvature perturbations $\mathcal{R}_k$ can be obtained as

$$\mathcal{R}_k'' + \frac{2z_s'}{z_s}\mathcal{R}_k' + c_s^2 k^2 \mathcal{R}_k = 0. \qquad (21)$$

The power spectrum of curvature perturbations is defined by

$$\mathcal{P}_{\mathcal{R}}(k) = \frac{k^3}{2\pi^2}|\mathcal{R}_k|^2, \qquad (22)$$

which is evaluated at the end of inflation using an exact numerical integration of the Fourier modes equation and by imposing the appropriate initial conditions on the Fourier modes in the subhorizon regime.

The linear tensor perturbations are described by the second-order action which is given by

$$\mathcal{S}_T^{(2)} = \frac{1}{8}\int dt d^3 x a^3 \left[\mathcal{G}_T \dot{h}_{ij}^2 - \frac{\mathcal{F}_T}{a^2}(\nabla h_{ij})^2\right], \qquad (23)$$

which in terms of conformal time can be written as,

$$\mathcal{S}_T^{(2)} = \int d\tau d^3 x z_T^2 \left(h_{ij}'^2 - c_T^2(\nabla h_{ij})^2\right), \qquad (24)$$

where $z_T = \frac{a}{2}(\mathcal{G}_T/2)^{1/2}$ and $c_T^2 = \mathcal{F}_T/\mathcal{G}_T$. Finally, the Fourier mode equation for tensor perturbations can be obtained by varying the above action which leads to

$$h_k'' + \frac{2z_T'}{z_T}h_k' + c_T^2 k^2 h_k = 0, \qquad (25)$$

and the power spectrum of tensor perturbations is defined by

$$\mathcal{P}_h(k) = 2\frac{k^3}{2\pi^2}|h_k|^2. \qquad (26)$$

Note that, the power spectra for both the scalar and tensor perturbations must be evaluated at the end of inflation or in the super-horizon limit $k/aH \ll 1$.

III. SOUND SPEED OF LINEAR PERTURBATIONS IN GNMDC AND CMB ANOMALIES

In this section, we shall discuss our approach to avoid the issues associated with the propagation speed of linear perturbations and instabilities that arise in the presence of the GNMDC term. In particular, we work in the regime of parameter space such that we avoid the problems like gradient instability and superluminal propagation of the scalar perturbations.

A. Sound speed of scalar perturbations

The propagation speed of the scalar modes in GNMDC setup is given by Eq. (13). Upon changing the time variable to the e-folds N using $dN = Hdt$ and defining $\phi_N = d\phi/dN$, $\phi_{NN} = d^2\phi/dN^2$, $H_N = dH/dN$, $\theta_N(\phi) = d\theta(\phi)/dN$, $g \equiv -\frac{1}{2}\theta(\phi)H^2$, and $h \equiv -\frac{1}{2}\theta_N(\phi)H^2$ together with some simplifications, we get

$$
\begin{aligned}
c_s^2 = & \Big(H(g\phi_N(\phi_N(g(18g + 8h + 1)\phi_N^2 - 4g + 8h + 2) + 16g\phi_{NN}(g\phi_N^2 + 1)) - 6g + 1) \\
& + 4gH_N(g\phi_N^2 + 1)(3g\phi_N^2 - 1)\Big)/\Big(H(g\phi_N^2 + 1)(g(18g + 1)\phi_N^2 - 6g + 1)\Big)
\end{aligned} \qquad (27)
$$

As we have discussed in the previous section, we are interested in generating features in the power spectrum due to the presence of the GNDMC term and thus, we assume that g and h need to be of $\mathcal{O}(1)$ or larger to get such large scale features. Moreover, if we also restrict ourselves to slowly varying functions of $\theta(\phi)$, we can assume[2] $|g| > |h| \gg H \gg |H_N|$ and $|g| > |h| \gg |\phi_N| > |\phi_{NN}|$. These imposed hierarchies are largely based on the requirement of having a stable inflationary phase and having a significant effect of the GNMDC term to generate localized features in the primordial power spectrum. Now, under these conditions and taking only the leading order contributions, it is possible to write c_s^2 as

$$c_s^2 \approx 1 - \frac{16g^2\phi_N^2}{1 - 6g} + \frac{16g^2\phi_N\phi_{NN}}{1 - 6g} + \frac{8gh\phi_N^2}{1 - 6g}. \qquad (28)$$

Since $|g| > \mathcal{O}(1)$ to get appropriate features in the scalar power spectra, the above expression further simplifies to

$$c_s^2 \approx 1 + \frac{8}{3}g\phi_N^2 - \frac{8}{3}g\phi_N\phi_{NN} - \frac{4}{3}h\phi_N^2 \approx 1 + \frac{8}{3}g\phi_N^2. \qquad (29)$$

---

[2]We have also numerically checked that these assumptions hold quite well for the entire duration of inflation.

For a consistent theory *sans* instabilities, we need $0 < c_s^2 \leq 1$, so from the above equation, it is evident that we need

$$0 \leq \theta(\phi) < \frac{3}{4\phi_N^2 H^2}. \tag{30}$$

Note that, while the first part $\theta(\phi) \geq 0$ is obtained to avoid the superluminal propagation of scalar perturbations, the second part of the above inequality, $\theta(\phi) < \frac{3}{4\phi_N^2 H^2}$ avoids the gradient instability, which is caused whenever the sound speed of scalar perturbations becomes imaginary. As studied in earlier works, the presence of such a gradient instability can cause an uncontrollable growth of scalar perturbation modes, thereby, rendering the theory inconsistent, even if the background evolution is stable [61,62]. It is, therefore, necessary to ensure that the squared sound speed of perturbation modes is always positive i.e. $c_s^2 > 0$.

B. Sound speed of tensor perturbations

Following the discussion of Sec. II, the sound speed of tensor perturbations is given by

$$c_T^2 = \frac{\mathcal{F}_T}{\mathcal{G}_T} = \frac{1 + X\theta(\phi)}{1 - X\theta(\phi)}. \tag{31}$$

As long as we work with negative values of $\theta(\phi)$, we can infer from the above equation that $c_T^2 < 1$, but any positive $\theta(\phi)$ shall lead to superluminal GWs. The recent detection of GWs from LIGO-VIRGO collaboration and their electromagnetic counterparts lead to a very stringent bound on the sound speed of GWs [63,64] given as,

$$-3 \times 10^{-15} < c_T - 1 < 7 \times 10^{-16}. \tag{32}$$

But it is to note that these bounds are valid for the late universe wherein the observed signals are originated. One can, in principle, argue that in very early universe, these bounds can be grossly violated.

C. Our adopted approach

While avoiding gradient instability constrains the amplitude of $\theta(\phi)$, and therefore the amplitude of local features in the scalar power spectra, the issue of superluminality for scalar and tensor modes is rather tricky to handle. To generate appropriate wiggles in the primordial scalar power spectrum, we use a localized dip of sufficient amplitude in the function $\theta(\phi)$. If we only consider this localized feature on top of the minimal setup, the local dip inevitably leads $\theta(\phi)$ to negative values. However, in the negative regime, $\theta(\phi)$ is constrained to be $\theta(\phi) > -1/9H^2$ from Eq. (8) for avoiding unphysical solutions. On the other hand, we need the amplitude of $\theta(\phi)$ to be of $\mathcal{O}(1/H^2)$ to obtain any visible features in power spectrum [56–58]. Considering

this difficulty, along with the restriction imposed by Eq. (30) to have subluminal propagation of scalar modes, we choose to restrict ourselves to positive values of $\theta(\phi)$. One immediate setback of this approach is to have super-luminal propagation of tensor modes. As is evident from Eq. (31), it is inevitable to have superluminal tensor modes whenever we consider $\theta(\phi) \geq 0$ regime. Equation (31) together with Eq. (30) shows that in these class of models which induce non-negligible features in the scalar power spectrum, superluminalities of scalar and tensor modes are mutually exclusive. In other words, the subluminal propagation of scalar modes requires $\theta(\phi) \geq 0$ which inevitably leads to superluminal GWs, and vice versa.

For the viability of our model, we restrict ourselves to the cases wherein we can completely avoid the gradient instability and superluminality for the scalar modes but the tensor models remain superluminal. To achieve this, we work with $\theta(\phi) > 0$ and propose a possible way to obtain $\theta(\phi) > 0$ throughout the evolution by using an extra monomial term in $\theta(\phi)$ which will be present during the inflationary phase but becomes negligible toward the end of inflation. Together with this, we have a local feature term that shall be active near the horizon exit of relevant large scales. In this case, the suppression or wiggles due to the local feature term will arise with respect to the amplification coming from the monomial term and not with respect to the minimal results. With this, we can now write,

$$\theta(\phi) = \theta_0(\phi) + \theta_1(\phi), \tag{33}$$

where $\theta_0(\phi)$ denotes the monomial term and $\theta_1(\phi)$ refers to the local term responsible for features in the spectrum. The advantage of using this setup is twofold. First, the monomial term $\theta_0(\phi)$ will cancel out any negative contribution coming from $\theta_1(\phi)$, and shall ensure that $\theta(\phi)$ is always positive for consistency. Second, it will also control the scalar spectral index n_s, and the tensor-to-scalar ratio r. In the context of primordial black holes forming models [65] and Higgs inflation [49], the applications of such monomial terms have been explored recently.

In Sec. IV A, we will discuss the choice of our $\theta(\phi)$, to obtain large-scale features in the primordial power spectrum. We show that by appropriate choice of a positive $\theta(\phi)$, we always reside in the subluminal regime for scalar modes, while tensor modes remain marginally superluminal during the inflationary evolution in our GNMDC setup. Figure 1 shows the extent of violation of the superluminality of tensors in terms of $c_T - 1$ for our best-fit GNMDC model, which is $\sim\mathcal{O}(10^{-11})$. Although this violates the bounds from Eq. (32), but as argued earlier, these bounds constrain the late universe physics, while the early inflationary phase can still have deviations from them.
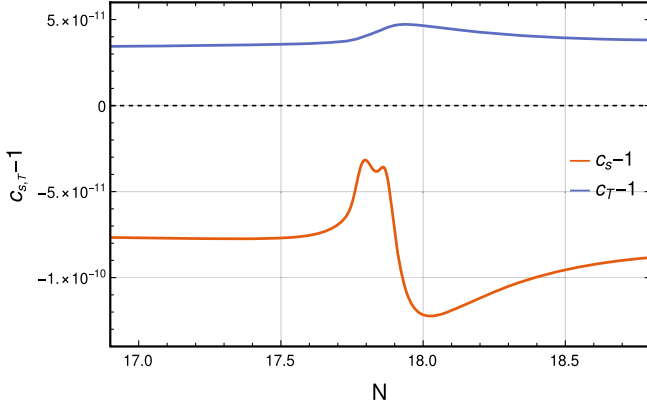
FIG. 1. The deviation of sound speed of scalar and tensor perturbations from unity in our GNMDC model for the best-fit parameter values of Dataset I as given in Table IV. As is evident from the plot, the scalar modes remain subluminal throughout, while the tensor modes are slightly superluminal in our GNMDC model. The sound speeds corresponding to the best-fit values from other datasets also show similar behavior.

IV. CHOICE OF THE GNMDC COUPLING FUNCTION AND INFLATIONARY MODELS

A. GNMDC coupling function $\theta(\phi)$

1. Choice of $\theta_0(\phi)$

The monomial term $\theta_0(\phi)$ is a global term that is dynamically active throughout the duration of inflation. The motivation to use this term is to ensure that $\theta(\phi)$ remains positive as we impose this condition following the discussion of our previous section. Further, to get an unaltered reheating history and the standard radiation domination, the contribution from this term should be negligible toward the end of inflation. Therefore, we essentially need a $\theta_0(\phi)$ term whose amplitude monotonically decreases during inflation. As a simple example, we work with a monomial form of $\theta_0(\phi)$ given as,

$$\theta_0(\phi) = A_0 \left(\frac{\phi}{\phi_i} \right)^n. \tag{34}$$

The sign of index n depends on the model for the potential of the inflaton field. For models where ϕ decreases with time, n should be positive so that by the end of inflation, GNMDC contribution becomes insignificant. Similarly, n should be negative for the potentials where ϕ increases with time. Previous studies have considered inflationary models with a monomial GNMDC term, leading to shifting in the values of n_s and r, in comparison to their values in the minimal setup without GNMDC. In Refs. [49,65], it has been shown that, for a given background model, such a monomial term with a larger index leads to a stronger shift in the values of n_s and r. In this work, we fix the power law index of $\theta_0(\phi)$, with $|n| = 4$, while its sign depends on the

potential of the inflationary model. Later in Sec. IV B, we will explore the behavior of different inflationary potentials $V(\phi)$ in the presence of such a monomial GNMDC term to find the best one with the allowed values of n_s and r. An appropriate combination of $V(\phi)$ and $\theta_0(\phi)$ leads to a nearly scale-invariant primordial power spectrum. Next, we will discuss the form of $\theta_1(\phi)$ in order to introduce desired localized features on the relevant large scales.

2. Choice of $\theta_1(\phi)$

The second term $\theta_1(\phi)$ is a local term whose effects would be significant only in the vicinity of the horizon exit of very large scales. While the monomial term $\theta_0(\phi)$ along with the background model of $V(\phi)$, sets the desired power law form of inflationary scalar power spectra, this local term is largely responsible for the superimposed oscillations on relevant scales. Previous studies [66–68] have suggested an overall suppression and superimposed oscillations at very large scales of inflationary scalar power spectra to explain the anomalies associated with the CMB temperature anisotropy power spectrum around multipoles $\ell \sim 20$–30. Therefore, to obtain such large-scale features, we propose a suitable form of the GNMDC function $\theta_1(\phi)$, such that it has a localized dip feature with a negative amplitude. In fact, a similar functional form of the coupling function has been used in [56], in the context of the formation of primordial black holes, where instead of a dip, a localized peak was introduced on relevant scales. In our work, we use

$$\theta_1(\phi) = -\frac{A_1}{\sqrt{1 + \frac{(\phi - \phi_0)^4}{\sigma}}}. \tag{35}$$

Here, A_1 is an overall amplitude factor, ϕ_0 represents the location of large-scale features, and σ effectively determines the width of the feature. In later sections, we shall compare this model with the data to arrive at the best-fit constraints on various parameters. The amplitude factor A_1 in Eq. (35) can be interpreted as

$$A_1 = A_{1,\mathrm{max}} \times f$$

where f is a fraction, with $0 \le f \le 1$. The quantity $A_{1,\mathrm{max}}$ is the maximum possible amplitude factor in $\theta_1(\phi)$, for a given A_0 [i.e., amplitude of $\theta_0(\phi)$] such that

$$\theta_0(\phi_{\mathrm{min}}) + \theta_1(\phi_{\mathrm{min}}) \ge 0,$$

where ϕ_{min} corresponds to the value of the scalar field at which $\theta_1(\phi)$ attains its minimum or the most negative value. This ensures that even at the most negative values of $\theta_1(\phi)$, the overall $\theta(\phi)$ still remains positive, following the discussion of Sec. III C. Note that, $f = 0$ implies the absence of any local diplike feature in the GNMDC

function, and hence the absence of any nontrivial large-scale features in the primordial power spectra. However, any nonzero value of f will induce suppression and superimposed oscillations in the power spectra on very large scales, where f controls the amplitude of these features. This will be discussed at length in the next section.

B. Choice of different inflationary potentials

As discussed in the introduction, in order to explain the large-scale CMB anomalies, we need appropriate scalar power spectra with superimposed oscillations from a given inflationary model. Specifically, to be consistent with the CMB constraints, we need (i) an appropriate amplitude A_s of the scalar power spectrum at the pivot scale [14] (ii) the correct value of the scalar spectral index n_s at the pivot scale [14] and, (iii) sufficiently low tensor to scalar ratio r so as to be consistent with the observational bound [14,16]. Moreover, in order to provide a better fit to the data, the power spectrum should have suppression at large scales and superimposed oscillations at intermediate scales [25,26,68,69].

In order to achieve these requirements, we have studied three different single-field inflationary models, in the presence of a GNMDC monomial term $\theta_0(\phi)$, to find the optimal one which satisfies all these conditions. We shall briefly discuss the advantages and disadvantages of these different models in the following subsections and finally work with the hilltop-quartic scenario for our analysis.

1. The quadratic model

One of the simplest models of inflation is described by the quadratic potential

$$V(\phi) = \frac{1}{2} m^2 \phi^2. \tag{36}$$

This large field model leads to a large tensor to scalar ratio $r \sim 0.1$ and has, therefore, been ruled out from recent Planck 2018 [14] and BICEP 2021 data release [16]. With the addition of a monomial GNMDC term $\theta_0(\phi)$ in the Lagrangian, it is possible to decrease r in this setup but that simultaneously increases the scalar spectral index n_s to quite a large value, far from the best fit and thus, fails to show any improvement with the CMB data. We study the behavior of the quadratic model together with the GNMDC monomial functional form $\theta_0(\phi) = A_0\phi^4$, where we vary the strength of the monomial term by varying the coefficient A_0. It is evident from Fig. 2 that even if we increase the strength of the monomial GNMDC term by increasing A_0, the quadratic model becomes strongly disfavored, particularly with the recent BICEP data [16], combined with the BAO observations.
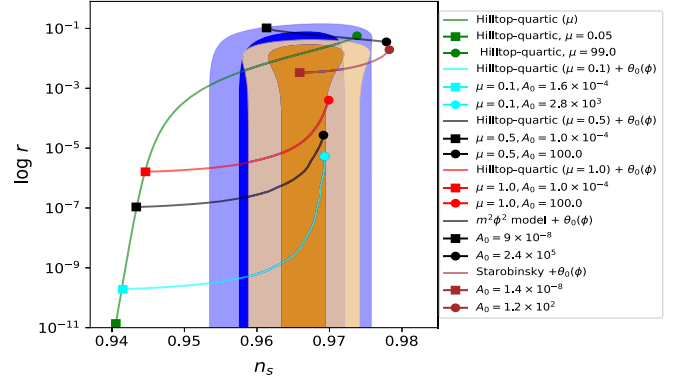

FIG. 2. The plot of n_s vs. r. The blue region indicates the 1-σ and 2-σ contours associated with the reference ΛCDM model with Planck data only while the yellow region indicates the 1-σ and 2-σ contours corresponding to the Planck + BICEP recent datasets. The predictions of various inflationary models have also been displayed on top of these contours. Among these scenarios, the Starobinsky model lies at the sweet spot of the observational constraints of Planck and BICEP data. Moreover, in the presence of the monomial GNMDC term characterized by an amplitude term A_0, we find that both the quadratic and Starobinsky model become disfavored with increasing A_0 while the hilltop-quartic model (for $\mu \lesssim 1$) provides a better fit with the data. This feature indicates that a class of models which are otherwise inconsistent with the observational constraints can possibly be made consistent with the data by introducing a monomial GNMDC term. For this reason, we finally use the hilltop-quartic model in our analysis.

2. The Starobinsky model

The potential for the Starobinsky model, in the Einstein frame, is given by

$$V(\phi) = V_0\left(1 - e^{-\sqrt{2/3}\phi/M_{\rm Pl}}\right)^2 \tag{37}$$

In the minimal setup, the Starobinsky model leads to the best-fit value of n_s and a very small value of r, thereby sitting at the so-called sweet spot of the Planck + BICEP allowed constraints. When we modify this minimal setup with the addition of a monomial GNMDC function with an appropriate amplitude, it inevitably shifts the values of both n_s and r from their optimal best-fit values. We study the Starobinsky setup in presence of the GNMDC monomial function of the form $\theta_0(\phi) = A_0\phi^4$, and as we can see from Fig. 2, increasing the strength of the monomial term leads to rendering the model inconsistent with the CMB observations. From our earlier discussion in Sec. III C, the presence of the monomial term in the GNMDC function is essential for a consistent model building and thus, we find that the Starobinsky model together with GNMDC is not a suitable scenario to work with.

3. The hilltop-quartic model

The hilltop inflationary scenarios are small field models in which inflation takes place near the maxima of the potential. These models are described by the potentials of the form

$$V(\phi) = V_0 \left[1 - \left(\frac{\phi}{\mu} \right)^p \right]. \tag{38}$$

According to Planck 2018 observations [14], the quartic potential ($p = 4$) provides a better fit to the data as compared to the quadratic potential ($p = 2$). Compared to the single-parameter models such as the quadratic or the Starobinsky model, this class of models is a two-parameter family of models which contain an extra parameter μ. In our setup, we start with the quartic potential with $p = 4$ and exploit the freedom of varying μ. This allows us comparatively large ranges for n_s and r, given that these models are well defined only in the limit $\phi < \mu$ [12].

As we can see in Fig. 2, in the minimal case, increasing μ simultaneously increases both n_s and r, and the scenario becomes consistent with the Planck + BICEP data only for $\mu \gg 1$. We further study the behavior of this model in the presence of a monomial GNMDC term $\theta_0(\phi)$. Since the hilltop quartic model belongs to the class of small field models, we work with a negative index of the monomial term, i.e., we choose $\theta_0(\phi) = A_0 \phi^{-4}$, following the arguments of Sec. IV A 1. The presence of this term shifts n_s to a higher value than its value in the minimal setup for a given μ by tuning A_0, as shown in Fig. 2. Thus, to get optimal values of n_s and r in the presence of $\theta_0(\phi)$, we need to start with μ which corresponds to a smaller value of n_s in the minimal setup. Henceforth, in our modified setup, we employ an extra advantage of the monomial GNMDC function, i.e., to fix the n_s issue, thereby making the hilltop-quartic scenario viable, even in the regime $\mu < 1$. It is evident from Fig. 2 that for small μ if we increase the amplitude of the monomial term, the value of n_s increases, but r does not show a significant increment, and we arrive at the optimal values for n_s and r which are consistent with the observational bounds of Planck + BICEP datasets.

Depending on the value of μ, the amplitude of the monomial term can be determined. The values of μ and $\theta_0(\phi)$ can be chosen appropriately to obtain the desired values of both n_s and r. It is important to note that, the hilltop-quartic model leads to a degeneracy between the potential parameter μ and the GNMDC parameter A_0, as is also evident from Fig. 2. It is possible to fix the value for any one of them while leaving the value of the other parameter to be determined from the best-fit parameter estimation methods. Moreover, this value will also depend on which datasets are being considered for the best-fit parameter estimation. For these values, the parameters of $\theta_1(\phi)$ can be adjusted such that $\theta(\phi) \equiv \theta_0(\phi) + \theta_1(\phi) > 0$. Finally, with these conditions in the GNMDC setup and staying consistent with the CMB data, one can obtain appropriate suppression and localized wiggles in the scalar power spectra.

V. DATA ANALYSIS SETUP AND METHODOLOGY

In this section, we shall discuss various details of our approach toward the numerical calculation of the primordial power spectrum, the methodology of our data analysis, and the details of the datasets that we use for obtaining the best-fit parameters constraints and the priors on various model parameters.

A. Primordial power spectrum

The GNMDC scenario discussed in the previous section brings about interesting and relevant oscillatory features in the primordial scalar power spectrum. In order to capture these oscillations precisely, we have developed a robust numerical code that solves the complex GNMDC equations for the evolution of the background and perturbation equations to yield the primordial scalar power spectrum. As discussed earlier, we employ the hilltop-quartic model as our base inflationary model. While the monomial term $\theta_0(\phi)$ broadly controls the value of n_s and r at the pivot scale, the localized GNMDC term, i.e., $\theta_1(\phi)$ is largely responsible for generating features i.e. strong dip/suppression together with superimposed localized oscillations on very large scales. Our scenario has inflationary potential parameters μ, V_0, and GNMDC parameters A_0, A_1, ϕ_0, and σ. Further, the maximum amplitude of the local GNMDC term A_1 is constrained to $A_{1,\mathrm{max}}$ from the requirement of an overall positive $\theta(\phi)$ as discussed in Sec. III C.

In our numerical module, we integrate all the background and perturbation equations exactly without incorporating any approximations. For the background evolution, we solve the Friedmann and Klein-Gordon equations using the slow roll initial conditions, following our discussion of Sec. II and appendix. This requires specifying only the initial value of the inflaton field i.e. $\phi_i = \phi(N = N_i)$ which is constrained by requiring that inflation lasts for a long enough duration. Further, to obtain the primordial power spectrum, we evolve the scalar perturbations from the subhorizon regime till they become frozen on the superhorizon scales and impose the standard Bunch-Davies vacuum initial conditions in the sub-Hubble regime $k \gg aH$. In all our numerical analyses, we ensure that we avoid the gradient instability and superluminality associated with the scalar perturbations. For the choice of the inflaton potential and the GNMDC coupling function in our setup, we find that the tensor perturbations remain exceedingly small ($r \sim 10^{-9}$) and thus, we do not take them into account in the data analysis. The three parameters viz. (ϕ_0, σ, A_1) of the local term $\theta_1(\phi)$, distinctively affect the location, width and the amplitude of the features in the
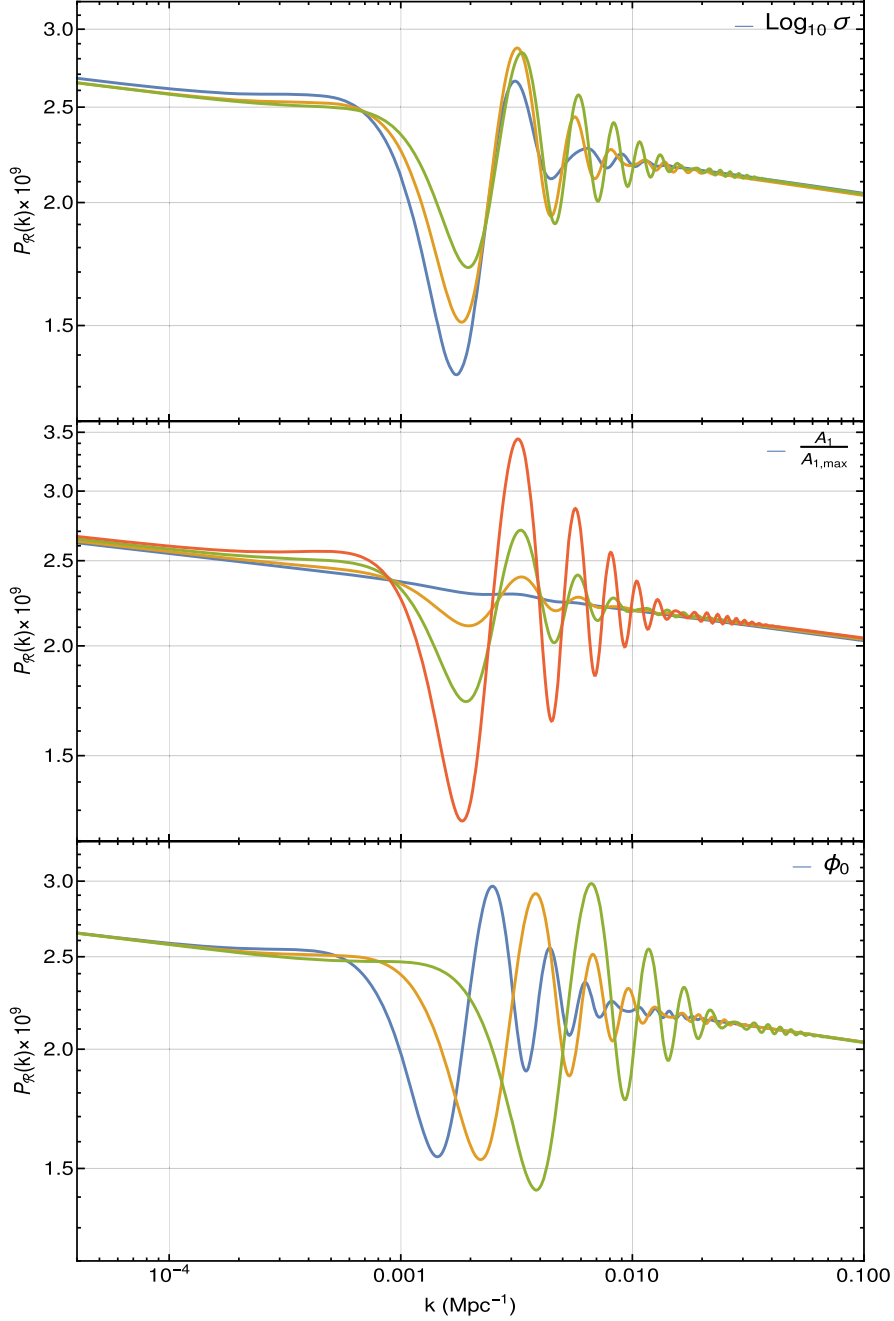
FIG. 3.   Primordial power spectrum of scalar perturbations for our model. For each of the panels, we have varied one parameter while keeping the other two fixed. These three parameters viz. (σ, A_1, ϕ_0) of the local term $\theta_1(\phi)$, distinctively affect the width, amplitude and the location of the features in the primordial power spectra, respectively. Note that, the GNMDC term is only responsible for generating such localized features in the spectrum. Away from the features, the spectrum is otherwise nearly scale-invariant or featureless. These localized superimposed oscillations do lead to a better fit to the data as compared to a nearly scale-invariant power spectrum.

primordial power spectra, respectively. A glimpse of the primordial power spectra of scalar perturbations obtained for different parameters of our model is shown in Fig. 3 and for each panel, we have varied one parameter while keeping the other two fixed.

As discussed earlier in Sec. IV B 3, there exists a degeneracy between the potential parameter μ and $\theta_0(\phi)$-parameter A_0. Thus, we fix the value of $\mu = 0.09M_{\text{Pl}}$

and vary A_0 to achieve optimal fitting from MCMC chains. This leaves us with five model parameters to sample: A_0, ϕ_0, A_1, σ, and V_0. The parameters V_0 and A_0 respectively fix the amplitude and the slope of the power spectrum around the pivot scale, ϕ_0 determines the location of the suppression and oscillations in the power spectra, σ localizes the features to the desired scales and A_1 controls the amplitude of the local GNMDC term.

B. Datasets used in our analysis

Heretofore, we have discussed the generation of large-scale features in the scalar power spectrum due to the GNMDC term and outlined various issues and their resolutions for consistent model building. The next step is to understand how such a model compare with the observational datasets and obtain the best-fit parameter constraints on the GNMDC parameters along with the background cosmological parameters. We use the latest release of the publicly available Planck 2018 CMB temperature and polarization (E-mode) anisotropy datasets [70]. Depending on the angular scales of interest and the distinguishable oscillatory features of a given model, one can choose the likelihoods provided by Planck for both small and large scales. Since our model primarily focuses on the CMB anomalies on the very large scales (low multipoles), we use the temperature and polarization likelihoods for these scales covering multipoles $\ell = 2$–29 in all the cases of our analysis. These likelihoods are `commander_dx12_v3_2_29` and `simall_100x143_offlike5_EE_Aplanck_B` for the temperature and polarization anisotropies, respectively. From now on, we will refer to them as `lowT` and `lowE`, where low indicates the low multipoles ($\ell = 2$–29), and T/E for temperature/polarization data respectively. To probe the features of our GNMDC model at higher multipoles (i.e., on smaller scales), we use the Planck official likelihoods named `plik_rd12_HM_v22_TT` and `plik_rd12_HM_v22b_TTTEEE` and we refer to them as `TT-Plik` and `TTTEEE-Plik` respectively. Furthermore, to test the robustness of our results, we also use the recent `Camspec-12.5HMcl` likelihoods for high-ℓ, which are obtained after reanalysis of the Planck 2018 data and span a slightly different range of multipoles. We refer to these as `TT-Camspec12.5` and `TTTEEE-Camspec12.5` respectively. We work with four dataset combinations which are listed in table I. These are `lowT+lowE+TT-Plik/Campec12.5` and `lowT+lowE+TTTEEE-Plik/Campsec12.5`, taking `lowT` and `lowE` common in all the cases.

C. Model parameters sampling

For a sampling of model parameters, we employ the publicly available code CosmoMC which performs a detailed Markov Chain Monte Carlo (MCMC) analysis so as to find the best-fit values of various model parameters. The choice

TABLE I. The four different likelihoods used in our analysis are characterized by four dataset combinations.

Datasets	Likelihoods used
Dataset I	lowT + lowE + TT-Plik
Dataset II	lowT + lowE + TTTEEE-Plik
Dataset III	lowT + lowE + TT-Camspec12.5
Dataset IV	lowT + lowE + TTTEEE-Camspec12.5

of working with the standard Metropolis Hasting sampling technique rather than nested sampling is due to the complicated numerical module to calculate the power spectrum in a GNMDC setup, which otherwise runs into difficulty when working with the latter. The code for calculating the CMB power spectrum, CAMB [71], is contained within CosmoMC which takes as input the background cosmological parameters including the parameters of the inflationary model, to yield the CMB temperature and polarization power spectra.

In the standard ΛCDM scenario which is our base reference model, there are six cosmological parameters $\Omega_b, \Omega_c, \tau, \Theta_s, A_s, n_s$ where the first four are baryon density, cold dark matter density, optical depth at reionization and sound horizon respectively, while the last two are the inflationary parameters; A_s setting the power spectrum normalization at the pivot scale and n_s determining the slope of the primordial scalar power spectrum. As we discussed earlier, in our set-up, instead of A_s and n_s, we have $V_0, A_0, A_1, \phi_0,$ and σ, and hence, a total of nine parameters, including four cosmological parameters. In order to generate the theoretical CMB power spectra for various model parameters, we couple our primordial power spectrum module to CAMB, such that it takes as input the GNMDC inflation model parameters along with the four background cosmological parameters.

In order to understand the improvement from our GNMDC inflationary scenario, we compare it with the reference ΛCDM models using CosmoMC with different datasets. The comparison is obtained in terms of the $\Delta\chi^2$ defined as $\Delta\chi^2 = \chi^2_{\Lambda\text{CDM}} - \chi^2_{\text{GNMDC}}$. To further find the true set of model parameters that best fit the observational data and the corresponding $\Delta\chi^2$, we use the likelihood maximizer algorithm BOBYQA [72] available in CosmoMC setup which further spans the parameter space, obtained after the MCMC sampling and identifies the better likelihood regions in our samples. Such a detailed analysis allows us to visualize the improvement in the fit coming from different scales in the power spectra. Finally, to correctly understand the improvement in the fit to each dataset, we write down the total $\Delta\chi^2$ as follows

$$\Delta\chi^2_{\text{total}} = \Delta\chi^2_{\text{lowT}} + \Delta\chi^2_{\text{lowE}} + \Delta\chi^2_{\text{high-}\ell} + \Delta\chi^2_{\text{prior}}. \quad (39)$$

In our analysis, we explicitly provide the variation of each of the terms with respect to the base ΛCDM model for all the four datasets that we have considered. Note that, the first three terms correspond to the improvement arising from the comparison with different datasets while $\Delta\chi^2_{\text{prior}}$ arises due to the priors on various model and nuisance parameters. These nuisance parameters are additional parameters contained in the high-ℓ likelihoods for calibration of the data.

TABLE II. The priors for the cosmological and model parameters used in our analysis. Note that, the range of priors remains the same for all four datasets.

Base and model parameters	Parameter	Priors
ΛCDM parameters	$\Omega_b h^2$	[0.005, 0.1]
	$\Omega_c h^2$	[0.001, 0.99]
	τ	[0.01, 0.8]
	$100\Theta_s$	[0.5, 10]
GNMDC parameters	A_0	[21.4, 22.0]
	ϕ_0/ϕ_i	[1.05, 1.055]
	$\log_{10}\sigma$	[−26.0, −24.0]
	$V_0 \times 10^{17}$	[5.9, 6.17]
	$A_1/A_{1,\text{max}}$	[0.01, 0.7]

D. Priors for the model parameters

The effective prior volume in the multidimensional parameter space which is sampled from the distribution during the CosmoMC analysis, is specified by the range of priors on various cosmological and model parameters. Moreover, the optimal range of priors also plays a crucial role in determining the best-fit values of various model parameters. For the case of our GNMDC scenario, the priors on various cosmological and model parameters are summarised in Table II. Among these, there are four base cosmological parameters, corresponding to the ΛCDM model and five model parameters, describing the GNMDC scenario. In Sec. V A, we have already discussed how these model parameters affect the location and amplitude of various features arising in the power spectrum. We choose these parameter priors carefully and appropriately such that we capture the essential features in the power spectrum and also do not inflate the prior volume of the parameter space else the convergence take a large amount of time. Further, in our analysis, the range of priors remains the same for all four data combinations as outlined in Table II.

VI. RESULTS

In this section, we shall present and discuss in detail the results of our analysis. These include the posterior distribution of the parameters obtained from the MCMC sampling using GetDist [73], the best-fit values of model parameters calculated using the BOBYQA routine, the detailed $\Delta\chi^2$ compared to the vanilla ΛCDM model with power-law power spectrum and finally, the best-fit residual CMB angular power spectra, showing significant improvement in fitting the Planck 2018 data. For all these cases, the MCMC runs are analyzed after the convergence is reached for all the chains based on the Gelman-Rubin convergence criteria [74] and we set $R - 1 \sim 0.05$ for all our chains analysis.

The results of our data analysis are shown in figure 4 wherein we display the 1D and 2D posterior distribution of the sampled model parameters for the dataset combinations `lowT+lowE+TT-Plik` and `lowT+lowE+TTTEEE-Plik`. As is evident from the figure, the posteriors for both datasets nearly overlap with each other for all the parameters. The posteriors also indicate that the data does not put strong constraints on all five parameters. However, the theoretical priors combined with the observational datasets seem to indicate a preferred value for some parameters. As evident from figure 4 and 5, only the parameters ϕ_0 and $A_1/A_{1,\text{max}}$ seem to be well constrained, with nearly closed contours.

The parameter ϕ_0, which determines the position of the prominent dip in the power spectrum, follows a near Gaussian profile, preferring a mean value corresponding to the diplike feature around multipoles $\ell \sim 20$–30, thereby improving the fit in the CMB temperature power spectrum on large scales. Next, the parameter $A_1/A_{1,\text{max}}$, which controls the amplitude of the localized GNMDC function, also admits a nonzero mean value indicating that the data indeed favors the presence of the local GNMDC term in our setup, which brings nontrivial features in the CMB power spectrum on relevant scales. The parameter σ, which controls the width of the feature, though shows a sharp peak corresponding to a preferred mean value but forms a rather scattered posterior. Further, the posteriors for the parameters A_0 and V_0, which collectively fix the values of n_s and r around the pivot scale, seem to be mostly prior bound. Indeed, there exists a degeneracy between V_0 and A_0, thereby, one can obtain better constraints on either of these, by fixing the other. For the case of `lowT+lowE+TT-Camspec12.5` and `lowT+lowE+TTTEEE-Camspec12.5`, we observe very similar behavior in the posterior distribution, as shown in Fig. 5. There also exists consistency in the best-fit constraints among all the datasets that we have considered in our analysis.

In Table III, we have listed the mean values of all the model parameters along with the background parameters together with 1-σ upper and lower bounds, from our data analysis for all four datasets. Although we have not listed the ΛCDM parameters explicitly, we do not find any significant shift in the background cosmological parameters in our analysis with respect to the ΛCDM model.

A. Best-fit values of model parameters and the CMB power spectrum

In order to obtain further improvement in the fit and the true best-fit values of model parameters, we use the BOBYQA routine for all four datasets. In Table IV, we have listed the best-fit results obtained from BOBYQA for all the five parameters. We found that the best-fit values differ slightly from each other for the parameters of our model. We further quote the obtained improvement in the fit, $\Delta\chi^2$, for individual likelihoods, as well as the total improvement,
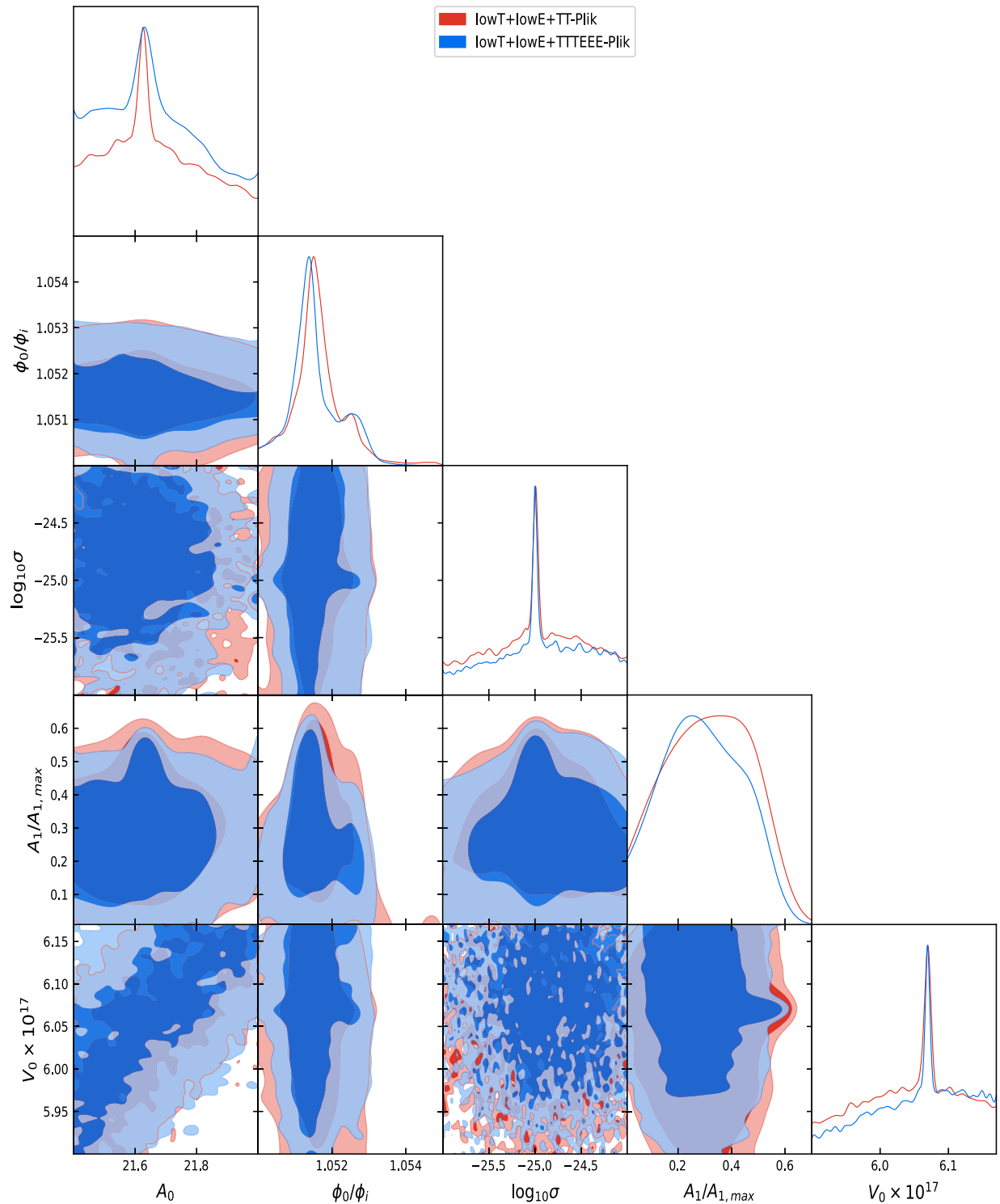
FIG. 4. The triangle plot of the 1D and 2D posterior distribution obtained from the COSMOMC sampling using the `lowT+lowE+TT-Plik` and `lowT+lowE+TTTEEE-Plik` likelihoods for the five model parameters of our GNMDC set-up (excluding the four cosmological parameters). The plot indicates that the data can place tight constraints on various model parameters.

in comparison to the base ΛCDM model with the power-law power spectrum.

As evident from Table IV for all four datasets, we get a significant improvement with $\Delta\chi^2 \sim 4.6$–5.3 from the lowT part, i.e., from the CMB temperature anisotropy data on low multipoles. This is what we targeted while choosing the toy model for $\theta_1(\phi)$, as the improvement mostly arises from the prominent dip in the primordial power spectra
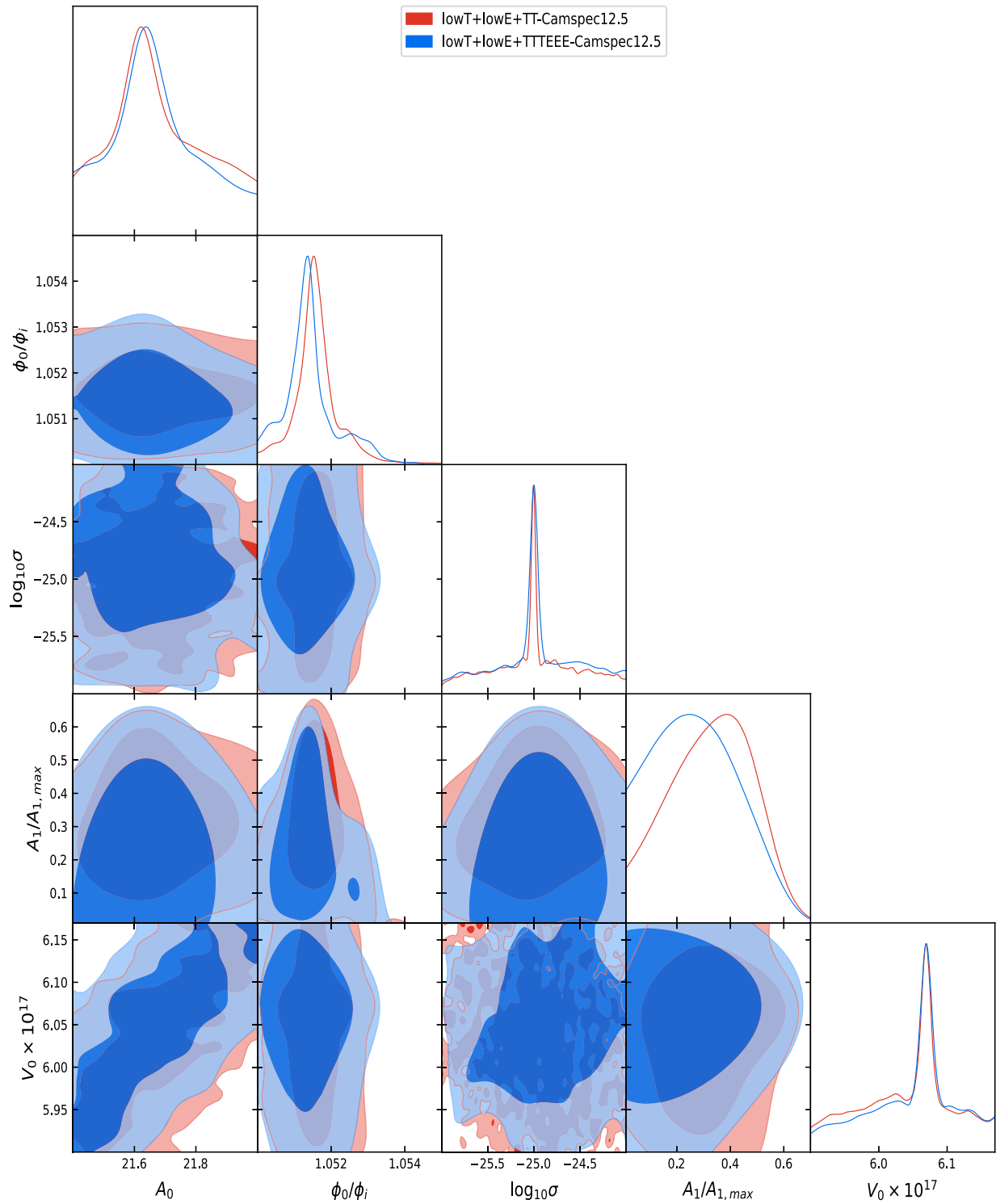
FIG. 5.   The triangle plot of the 1D and 2D posterior distribution obtained from the COSMOMC sampling using the `lowT+lowE+TT-Camspec12.5` and `lowT+lowE+TTTEEE-Camspec12.5` likelihoods for the five model parameters for our GNMDC set-up (excluding the four cosmological parameters). The plot indicates that the data can provide stringent constraints on various model parameters.

corresponding to large scales caused due to $\theta_1(\phi)$ term. There is no significant improvement coming from the lowE polarization anisotropy data, indicating that the data is merely sensitive to the modifications in the power spectra introduced in our setup. In our best-fit samples, a small improvement to the fit on smaller scales (large multipoles)

TABLE III.   We present the best-fit constraints on various model parameters from the MCMC analysis of the GNMDC scenario for four dataset combinations. The mean values of all the parameters along with their 1-σ constraints are listed here. We find that the best-fit values of model parameters are very close to each other for all the different datasets and likelihood combinations.

Parameters	Dataset I	Dataset II	Dataset III	Dataset IV
$\Omega_b h^2$	0.02219 ± 0.00017	0.02238 ± 0.00013	0.02220 ± 0.00019	0.02225 ± 0.00013
$\Omega_c h^2$	0.1200 ± 0.0010	0.12022 ± 0.00084	0.1194 ± 0.0013	0.11998 ± 0.00099
τ	0.0535 ± 0.0061	0.0541 ± 0.0059	$0.0537^{+0.0062}_{-0.0051}$	$0.0536^{+0.0059}_{-0.0051}$
$100\Theta_s$	1.04087 ± 0.00041	1.04091 ± 0.00030	1.04078 ± 0.00040	1.04102 ± 0.00027
A_0	$21.666^{+0.089}_{-0.24}$	$21.659^{+0.078}_{-0.25}$	$21.68^{+0.14}_{-0.18}$	$21.67^{+0.13}_{-0.16}$
ϕ_0/ϕ_i	$1.05164^{+0.00047}_{-0.00072}$	$1.0516^{+0.0011}_{-0.00074}$	$1.05161^{+0.00040}_{-0.00057}$	$1.05146^{+0.00045}_{-0.00078}$
$\log_{10}\sigma$	-24.96 ± 0.50	$-24.93^{+0.81}_{-0.39}$	-24.99 ± 0.46	-24.96 ± 0.45
$V_0 \times 10^{17}$	$6.047^{+0.092}_{-0.059}$	> 6.04	$6.043^{+0.063}_{-0.076}$	$6.050^{+0.060}_{-0.072}$
$A_1/A_{1,\max}$	$0.32^{+0.18}_{-0.16}$	0.30 ± 0.15	$0.33^{+0.17}_{-0.14}$	$0.28^{+0.13}_{-0.20}$

TABLE IV.   The best-fit constraints on various model parameters obtained after the `BOBYQA` analysis for the different likelihood combinations. The bottom rows also list each contribution in $\Delta\chi^2$ compared to the reference ΛCDM model and finally, the net improvement $\Delta\chi^2_{\mathrm{total}}$ for our scenario corresponding to different datasets.

Parameters	Dataset I	Dataset II	Dataset III	Dataset IV
A_0	21.5599	21.5858	21.6669	21.6008
ϕ_0/ϕ_i	1.0515	1.0513	1.0515	1.0513
$\log_{10}\sigma$	-25.5429	-24.9896	-25.1201	-24.7700
$V_0 \times 10^{17}$	5.9805	6.0604	6.0265	6.0072
$A_1/A_{1,\max}$	0.4770	0.4052	0.4743	0.3547
$\Delta\chi^2_{\mathrm{lowT}}$	5.3080	4.6490	5.0740	4.6220
$\Delta\chi^2_{\mathrm{lowE}}$	-0.0110	-0.5880	-0.1160	-0.1250
$\Delta\chi^2_{\mathrm{high}\text{-}\ell}$	1.27	1.90	2.3310	0.8140
$\Delta\chi^2_{\mathrm{prior}}$	-0.1133	0.1596	-0.4145	0.0036
$\Delta\chi^2_{\mathrm{total}}$	6.4537	6.1206	6.8745	5.3146

is also seen, $\Delta\chi^2 \sim 0.8$–2.3 for all four datasets. These features on smaller scales in the CMB data can be attributed to the decaying oscillatory features in the primordial power spectra following the most prominent dip, as also seen in Fig. 3. Although we mentioned that the improvement on smaller scales is not as significant, since the features in the power spectra are obtained to primarily focus on anomalies on large scales. Indeed, by some other suitable choice of coupling function $\theta_1(\phi)$, which induces small oscillations on relatively smaller scales in the power spectrum similar to [66,75], one can obtain significant improvement from these scales too. Further the χ^2_{prior} which arises from the nuisance parameters for the likelihoods is nearly the same as that of the reference model. Finally, in terms of the overall improvement, we find that $\Delta\chi^2_{\mathrm{total}} \sim 5.3$–$6.8$ and the maximum improvement in $\Delta\chi^2_{\mathrm{total}} \sim 6.8$ is obtained for the dataset `lowT+lowE+TT-Camspec12.5`. On a final note, in all four dataset combinations, the dominant improvement in $\Delta\chi^2_{\mathrm{total}}$ comes from the low multipole

temperature anisotropies data, indicating that the modifications introduced in the primordial power spectrum in our setup, are well accommodated by the anomalous features in CMB on low multipoles ($\ell < 30$). This summarizes the best-fit improvement obtained for the GNMDC model that we have considered in our analysis.

It might be very interesting to explore other coupling functions within the GNMDC setup which might lead to an even better improvement in the lowT regime, e.g., due to a suppressed power spectrum on very low multipoles so as to address the low quadrupole anomaly in the CMB as well as lead to other characteristic modulations at higher multipoles to get even better fit from the high-ℓ data.

In Fig. 6, we plot the scalar power spectra for the best-fit values of model parameters obtained after the `BOBYQA` analysis for all four datasets combinations. While the broad behavior of the features in the spectra (a broad dip followed by localized superimposed oscillations) remains the same, the different datasets still suggest a slight difference in the
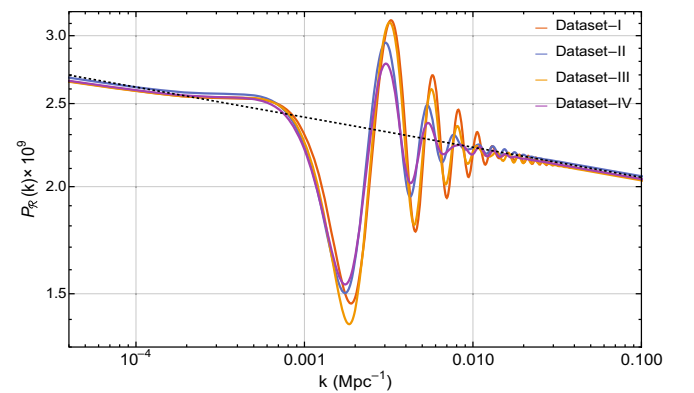

FIG. 6.   The scalar power spectra are plotted for the best-fit values of our GNMDC model parameters obtained after the `BOBYQA` analysis, along with a nearly scale-invariant spectrum for the best-fit values of A_s and n_s (in dashed). While the global features in the spectra remain the same, the different datasets seem to prefer these localized modulations with slightly different magnitudes and locations.

location and amplitude of these features. Away from these localized features, the power spectra reduce to a nearly scale-invariant power spectrum, as evident from the Fig. 6. It is interesting to point out that these features strongly resemble the features obtained in a canonical single field inflationary model with the introduction of a step in the inflaton potential [25,27,76]. Needless to say, our GNMDC scenario offers a new and interesting possibility to generate such large-scale features in the spectrum to prove to be a better fitting model to the CMB observations. It will be interesting to examine if the oscillatory features arising

in our model also provide a resolution to the lensing anomaly [77,78].

Further, to understand the resulting imprints in the CMB, we have plotted the residual CMB angular power spectra ΔD_ℓ^{TT}, ΔD_ℓ^{TE}, and ΔD_ℓ^{EE} corresponding to the best-fit values of the model parameters for all the four datasets which are displayed in Fig. 7. The top panel in this figure corresponds to datasets I and II, while the lower is plotted for the datasets III and IV. It is evident from this figure that all these best-fit CMB spectra show similar features. Our GNMDC scenario is not able to address the
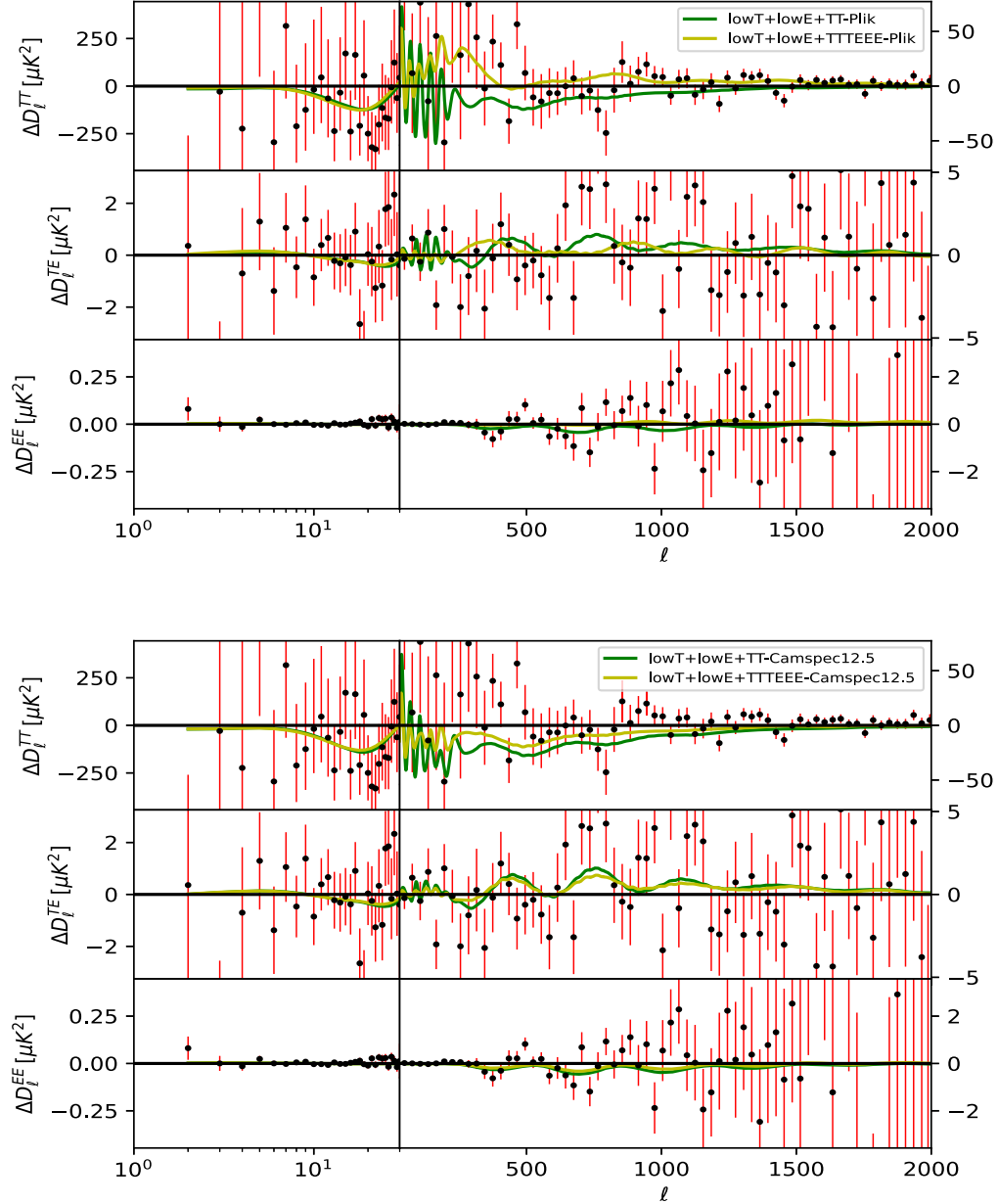

FIG. 7. The residual CMB angular power spectra are plotted for our GNMDC scenario with respect to the base ΛCDM model, corresponding to the best-fit parameters obtained from BOBYQA analysis for all the four datasets (mentioned in table IV). The improvement arising from the low-ℓ regime turns out to be more significant than the high-ℓ regime.

low quadrupole. Still, it results in oscillatory features around $\ell \sim 20$–30, which improves the overall fit in the low-ℓ regime as compared to the base featureless model. Further, we do not get any significant improvement in the E-mode polarization autocorrelation data (D_ℓ^{EE}), suggesting that such a setup may not improve the fit to the same beyond the standard model. Notably, the improvement arising from the high-ℓ regime seems to somewhat differ from each other for all four datasets. Our scenario does generate tiny small-scale features but not as relevant and prominent as the clock signals, discussed in [66,68]. We close this section with an interesting prospect that the class of GNMDC models that we have considered in this work, hold the promise of being viable alternatives of primordial feature models, and they can be further expanded by considering different forms of the GNMDC functions as well as other mechanisms to generate prominent small scale features.

VII. CONCLUSIONS AND DISCUSSIONS

Precision observations of CMB anisotropies over the last few decades are one of the most outstanding achievements of modern cosmology. These anisotropies contain crucial information about the evolution of the universe at the earliest epochs, particularly during the inflationary phase. Although the present observational data strongly favor the standard ΛCDM model as the concordance model of the universe, various anomalies present in the CMB data may nevertheless hint at some new primordial physics beyond the standard model of cosmology. Interestingly, these large-scale anomalies have always been present in the CMB observations from COBE, and WMAP to the most recent and precise Planck datasets, which makes them more intriguing to look at and understand their origins better. While they could arise due to foreground residuals and/or systematic effects, their origin could also be primordial, which could point toward nontrivial dynamics beyond the simplest inflationary models, which typically lead to a nearly scale-invariant power spectrum on all scales.

In this paper, we have studied the cosmological implications of the GNMDC term that arises within the framework of Horndeski theories and explored whether large-scale features in the CMB can be generated in this scenario. Since the evolution of background and perturbations is quite involved in this model, we have developed an accurate numerical module to compute the primordial spectra of scalar and tensor perturbations. Further, we have compared our model with the CMB anisotropies data from Planck in temperature (TT), E-mode polarization (EE), and their cross-correlation (TE) and explored the parameter space to find out the best-fit values of various model parameters. We found that this class of models can indeed generate large-scale features in the CMB angular power spectra for a specific choice of the GNMDC function and provide an improvement over the reference ΛCDM model

with a featureless power-law primordial spectrum. The CMB angular power spectrum corresponding to the best-fit parameters indicates that the dominant improvement primarily arises from the low-ℓ region with marginal improvement from the high-ℓ region. To our knowledge, this is the first time that such models have been employed to understand the origin of large-scale features in the CMB angular power spectrum. Our results demonstrate the possibility of explaining large-scale features in the CMB by going beyond the canonical scalar field models without any additional features in the inflaton potential but within the single field inflationary framework.

The GNMDC scenario offers a richer phenomenology in terms of freedom to choose the form of the coupling function. Hence, it might be interesting to explore if these models can also explain the presence of other feature anomalies in the CMB, e.g., low quadrupole suppression and peculiar clock features at smaller scales. As discussed earlier, from a theoretical perspective, a model can be a consistent physical model only if it avoids the gradient and Ostrogradsky instabilities. However, from a statistical perspective, a model can be termed a better alternative only if it improves the fit to the data compared to a reference model. Needless to say, a preferable scenario would be the one that provides a satisfactory explanation to multiple anomalies in the CMB observations and also proves to be a significantly better fit to the data at the expense of fewer additional parameters. Within this GNMDC framework, it will also be helpful to work with different choices of the coupling function leading to suitable oscillations on smaller scales which can provide a better improvement arising from smaller scales. In addition to the CMB anisotropies data from Planck, large-scale features in the power spectrum can, in principle, also be independently constrained by the large-scale structure (LSS) observations of galaxy surveys as the primordial features also leave distinct imprints in the matter power spectrum, as evident from figure 8. However, localized features on scales larger than $k \sim 0.01 \ h \,\mathrm{Mpc}^{-1}$ may not be constrained by the LSS data while features on smaller scales or running features on all scales can be independently constrained by the LSS observations [79–88]. Upcoming LSS surveys such as Euclid and LSST should be able to provide better constraints on such primordial spectral features [89,90]. Thus, LSS observations can be used as a complementary probe along with the CMB data to constrain nontrivial features in the power spectra and the deviations from scale invariance on sub-CMB scales. Moreover, future 21-cm tomographic observations also have enormous potential to constrain such primordial features to a great extent [91–93]. In addition, spectral distortions of the CMB power spectrum provide an entirely complementary window on the scale dependence of the primordial power spectrum and small-scale features since they strongly depend on the spectral amplitude at
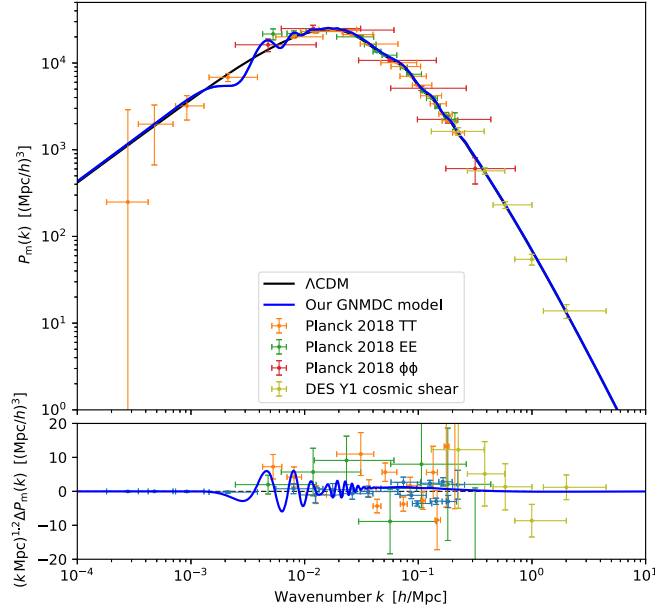
FIG. 8. The linear matter power spectrum at $z = 0$ (top) and the residuals (below) for our scenario for the best-fit values of model parameters. Precise LSS observations contain the enormous potential to constrain features in the spectrum independently but not the features on very large scales as those scales remain inaccessible by LSS [96].

scales smaller than LSS. Future experiments such as PIXIE [94] or PRISM [95] should be able to provide interesting constraints on departures from a featureless primordial power spectrum. All these observations from CMB, LSS, 21-cm, and spectral distortions prove to be complementary. Together, they will provide stringent constraints on the primordial power spectrum over a wide range of scales.

Primordial non-Gaussianity (PNG) is also an important probe that can provide independent constraints on the scale dependence of the power spectrum. In particular, inflationary models with features in the power spectrum are well known to generate correlated signatures in PNG [97–102]. Therefore, present and future PNG constraints from CMB and LSS can constrain these feature models better. Near future CMB experiments aimed at precise measurements of CMB E- and B-mode polarization such as CMB-S4 [103], LiteBIRD [104,105], Simons Observatory (SO) [106,107]

and CMB-Bharat [108] should also be able to provide relevant constraints on the small scale dynamics of inflationary models with features and their cross-correlations with other probes should further tighten the parameter constraints. With the availability of future precise data, many consistent models may be ruled out or strongly constrained. The prospects of a better understanding of the interconnection between primordial spectral features and underlying physics will undoubtedly be improved. Therefore, future cosmological observations offer an exciting promise to constrain the primordial universe better.

ACKNOWLEDGMENTS

APPENDIX: GNMDC EQUATIONS FOR BACKGROUND AND PERTURBATIONS

In this appendix, we present the GNMDC equations for the background evolution and the scalar and tensor perturbations in terms of e-folds N, which we employ in our numerical code.

1. Background equations

The Friedmann equations for our GNMDC setup, as given in Eqs. (4) and (5), can be written in terms of N as

$$3H^2 = \kappa^2 \left[\frac{1}{2} H^2 \phi_N^2 (9H^2 \theta(\phi) + 1) + V(\phi) \right], \qquad \text{(A1)}$$

$$-2HH_N = \kappa^2 \left[(1 + 3\kappa^2 \theta(\phi)H^2 - \kappa^2 \theta(\phi)HH_N)H^2 \phi_N^2 - \kappa^2 \theta'(\phi)H^4 \phi_N^3 - 2\kappa^2 \theta(\phi)H^2 \phi_N (H^2 \phi_{NN} + HH_N \phi_N) \right], \qquad \text{(A2)}$$

and the Klein-Gordon equation becomes

$$[1 + 3H^2 \theta(\phi)](H^2 \phi_{NN} + HH_N \phi_N) + 3H^2 \phi_N [(3H^2 + 2HH_N)\theta(\phi) + 1] + \frac{3}{2} H^4 \phi_N^2 \theta'(\phi) + V'(\phi) = 0, \qquad \text{(A3)}$$

where $\phi_N = d\phi/dN$, $\phi_{NN} = d^2\phi/dN^2$, $H_N = dH/dN$ and $\theta'(\phi) = d\theta(\phi)/d\phi$. We set $\kappa = 1$ in our numerical code.

2. Scalar and tensor perturbations

The Mukhanov-Sasaki equation for the Fourier modes of curvature perturbations $\mathcal{R}_k$, as given in Eq. (21), can be further written in terms of N as follows

$$\frac{d^2\mathcal{R}_k}{dN^2} + \left(1 + \frac{H_N}{H} + \frac{2z_{s_N}}{z_s}\right)\frac{d\mathcal{R}_k}{dN} + \left(\frac{k^2c_s^2}{a^2H^2}\right)\mathcal{R}_k = 0. \tag{A4}$$

Here, $z_{s_N} = dz_s/dN$ and c_s^2 and z_{s_N}/z_s are given by

$$c_s^2 = \frac{1}{((H^2\theta(\phi)\phi_N^2 - 2)(9H^4\theta(\phi)^2\phi_N^2 - H^2\theta(\phi)(\phi_N^2 - 6) + 2)^2)}[H^4\theta(\phi)^3\phi_N^2(-6H^4\phi_N^5\theta'(\phi) + H^2(3\phi_N^4 - 244\phi_N^2 + 420)$$
$$- 48\phi_N V'(\phi)) + 2\theta(\phi)^2(12H^6\phi_N^5\theta'(\phi) + 24H^2\phi_N V'(\phi) + H^4(-7\phi_N^4 + 100\phi_N^2 - 36))$$
$$- 4H^2\theta(\phi)(6H^2\phi_N^3\theta'(\phi) - 5\phi_N^2 + 12) + 6H^6\theta(\phi)^4\phi_N^4(13H^2(\phi_N^2 - 9) + 2\phi_N V'(\phi)) + 351H^{10}\theta(\phi)^5\phi_N^6 - 8]$$

$$\frac{z_{s_N}}{z_s} = \frac{1}{(H^2\phi_N(H^2\phi_N^2\theta(\phi) - 2)(3H^2\phi_N^2\theta(\phi) - 2)(9H^4\phi_N^2\theta(\phi)^2 - H^2(\phi_N^2 - 6)\theta(\phi) + 2)^2)}[H^2\phi_N(3H^8\phi_N^4\theta(\phi)^3(\phi_N^5\theta'(\phi)$$
$$+ (-20\phi_N^4 + 54\phi_N^2 + 936)\theta(\phi)). - H^6\phi_N^2\theta(\phi)^2(2(5\phi_N^2 + 24)\phi_N^3\theta'(\phi) + (3\phi_N^6 - 220\phi_N^4 - 132\phi_N^2 + 720)\theta(\phi))$$
$$+ 2H^4\theta(\phi)(2(\phi_N^2 + 24)\phi_N^3\theta'(\phi) + (7\phi_N^6 - 132\phi_N^4 + 60\phi_N^2 - 144)\theta(\phi)) - 4H^2((5\phi_N^4 - 36\phi_N^2 + 48)\theta(\phi) - 2\phi_N^3\theta'(\phi))$$
$$+ 972H^{12}\phi_N^8\theta(\phi)^6 + 27H^{10}\phi_N^6(\phi_N^2 - 84)\theta(\phi)^5 + 8(\phi_N^2 - 4)) + V'(\phi)(27H^{10}\phi_N^8\theta(\phi)^5 - 9H^8\phi_N^6(\phi_N^2 + 12)\theta(\phi)^4$$
$$+ 8H^6\phi_N^4(5\phi_N^2 + 24)\theta(\phi)^3. - 8H^4\phi_N^2(7\phi_N^2 + 18)\theta(\phi)^2 + 16H^2(2\phi_N^2 - 3)\theta(\phi) - 16)] \tag{A5}$$

The Fourier mode equation for the tensor perturbations h_k in terms of N can be written as

$$\frac{d^2h_k}{dN^2} + \left(1 + \frac{H_N}{H} + \frac{2z_{T_N}}{z_T}\right)\frac{dh_k}{dN} + \left(\frac{c_T^2 k^2}{a^2 H^2}\right)h_k = 0, \tag{A6}$$

where

$$c_T^2 = \frac{1 + H^2\theta(\phi)\phi_N^2/2}{1 - H^2\theta(\phi)\phi_N^2/2} \tag{A7}$$

and

$$\frac{z_{T_N}}{z_T} = \frac{1}{(2(H^2\theta(\phi)\phi_N^2 - 2)(9H^4\theta(\phi)^2\phi_N^2 - H^2\theta(\phi)(\phi_N^2 - 6) + 2))}[2H^2(\phi_N^3\theta'(\phi) + \theta(\phi)^2\phi_N^3 V'(\phi) - 2\theta(\phi)(\phi_N^2 + 6))$$
$$+ H^4\theta(\phi)\phi_N^2(4\theta(\phi)(4\phi_N^2 - 15) - \phi_N^3\theta'(\phi)) + 72H^6\theta(\phi)^3\phi_N^4 - 4(\theta(\phi)\phi_N V'(\phi) + 2)].$$

As mentioned earlier, the mode equation (A4) for $\mathcal{R}_k$ is evolved for each Fourier mode with the Bunch-Davies initial conditions imposed on $\mathcal{R}_k$ and its derivative when the modes are deep inside the horizon (subhorizon regime, i.e., $k/aH \gg 1$). In terms of conformal time τ, we can write

$$\mathcal{R}_k(\tau)|_{k \gg aH} = \frac{1}{z_s}\frac{e^{-ic_s k\tau}}{\sqrt{2c_s k}}.$$

Similarly, the Bunch-Davies initial conditions for the tensors on h_k are similar to those of scalars with $c_s \to c_T$ and $z_s \to z_T$.

[1] A. A. Starobinsky, A new type of isotropic cosmological models without singularity, Phys. Lett. **91B,** 99 (1980).

[2] A. H. Guth, The inflationary universe: A possible solution to the horizon and flatness problems, Phys. Rev. D **23,** 347 (1981).

[3] A. D. Linde, A new inflationary universe scenario: A possible solution of the horizon, flatness, homogeneity, isotropy and primordial monopole problems, Phys. Lett. **108B,** 389 (1982).

[4] A. Albrecht and P. J. Steinhardt, Cosmology for Grand Unified Theories with Radiatively Induced Symmetry Breaking, Phys. Rev. Lett. **48,** 1220 (1982).

[5] A. D. Linde, Chaotic inflation, Phys. Lett. **129B,** 177 (1983).

[6] A. A. Starobinsky, Spectrum of relict gravitational radiation and the early state of the universe, JETP Lett. **30,** 682 (1979).

[7] V. F. Mukhanov and G. V. Chibisov, Quantum fluctuations and a nonsingular universe, JETP Lett. **33,** 532 (1981).

[8] M. Tegmark, What does inflation really predict?, J. Cosmol. Astropart. Phys. 04 (2005) 001.

[9] B. A. Bassett, S. Tsujikawa, and D. Wands, Inflation dynamics and reheating, Rev. Mod. Phys. **78,** 537 (2006).

[10] D. Baumann, Inflation, in *Physics of the Large and the Small* (World Scientific, Singapore, 2011), pp. 523.

[11] L. Sriramkumar, An introduction to inflation and cosmological perturbation theory, arXiv:0904.4584.

[12] J. Martin, C. Ringeval, and V. Vennin, Encyclopædia inflationaris, Phys. Dark Universe **5–6,** 75 (2014).

[13] G. Hinshaw *et al.* (WMAP Collaboration), Nine-year Wilkinson microwave anisotropy probe (WMAP) observations: Cosmological parameter results, Astrophys. J. Suppl. Ser. **208,** 19 (2013).

[14] Y. Akrami *et al.* (Planck Collaboration), Planck 2018 results. X. Constraints on inflation, Astron. Astrophys. **641,** A10 (2020).

[15] Y. Akrami *et al.* (Planck Collaboration), Planck 2018 results. IX. Constraints on primordial non-Gaussianity, Astron. Astrophys. **641,** A9 (2020).

[16] P. A. R. Ade *et al.* (BICEP, Keck Collaborations), Improved Constraints on Primordial Gravitational Waves using Planck, WMAP, and BICEP/Keck Observations through the 2018 Observing Season, Phys. Rev. Lett. **127,** 151301 (2021).

[17] M. R. Nolta *et al.* (WMAP Collaboration), Five-year Wilkinson microwave anisotropy probe (WMAP) observations: Angular power spectra, Astrophys. J. Suppl. Ser. **180,** 296 (2009).

[18] D. J. Schwarz, C. J. Copi, D. Huterer, and G. D. Starkman, CMB Anomalies after Planck, Classical Quantum Gravity **33,** 184001 (2016).

[19] Y. Akrami *et al.* (Planck Collaboration), Planck 2018 results. VII. Isotropy and Statistics of the CMB, Astron. Astrophys. **641,** A7 (2020).

[20] J. Chluba, J. Hamann, and S. P. Patil, Features and new physical scales in primordial observables: Theory and observation, Int. J. Mod. Phys. D **24,** 1530023 (2015).

[21] A. Slosar *et al.*, Scratches from the past: Inflationary archaeology through features in the power spectrum of primordial fluctuations, Bull. Am. Astron. Soc. **51,** 98 (2019).

[22] J. A. Adams, B. Cresswell, and R. Easther, Inflationary perturbations from a potential with a step, Phys. Rev. D **64,** 123514 (2001).

[23] P. Hunt and S. Sarkar, Multiple inflation and the WMAP "glitches", Phys. Rev. D **70,** 103518 (2004).

[24] P. Hunt and S. Sarkar, Multiple inflation and the WMAP glitches. 2. Data analysis and cosmological parameter extraction, Phys. Rev. D **76,** 123504 (2007).

[25] L. Covi, J. Hamann, A. Melchiorri, A. Slosar, and I. Sorbera, Inflation and WMAP three year data: Features have a Future!, Phys. Rev. D **74,** 083509 (2006).

[26] J. Hamann, L. Covi, A. Melchiorri, and A. Slosar, New constraints on oscillations in the primordial spectrum of inflationary perturbations, Phys. Rev. D **76,** 023503 (2007).

[27] D. K. Hazra, M. Aich, R. K. Jain, L. Sriramkumar, and T. Souradeep, Primordial features due to a step in the inflaton potential, J. Cosmol. Astropart. Phys. 10 (2010) 008.

[28] A. Ashoorioon, C. van de Bruck, P. Millington, and S. Vu, Effect of transitions in the Planck mass during inflation on primordial power spectra, Phys. Rev. D **90,** 103515 (2014).

[29] P. Hunt and S. Sarkar, Search for features in the spectrum of primordial perturbations using Planck and other datasets, J. Cosmol. Astropart. Phys. 12 (2015) 052.

[30] I. Dalianis, G. P. Kodaxis, I. D. Stamou, N. Tetradis, and A. Tsigkas-Kouvelis, Spectrum oscillations from features in the potential of single-field inflation, Phys. Rev. D **104,** 103510 (2021).

[31] R. K. Jain, P. Chingangbam, and L. Sriramkumar, On the evolution of tachyonic perturbations at super-Hubble scales, J. Cosmol. Astropart. Phys. 10 (2007) 003.

[32] R. K. Jain, P. Chingangbam, J.-O. Gong, L. Sriramkumar, and T. Souradeep, Punctuated inflation and the low CMB multipoles, J. Cosmol. Astropart. Phys. 01 (2009) 009.

[33] R. K. Jain, P. Chingangbam, L. Sriramkumar, and T. Souradeep, The tensor-to-scalar ratio in punctuated inflation, Phys. Rev. D **82,** 023509 (2010).

[34] M. H. Qureshi, A. Iqbal, M. A. Malik, and T. Souradeep, Low-ℓ power suppression in punctuated inflation, J. Cosmol. Astropart. Phys. 04 (2017) 013.

[35] C. R. Contaldi, M. Peloso, L. Kofman, and A. D. Linde, Suppressing the lower multipoles in the CMB anisotropies, J. Cosmol. Astropart. Phys. 07 (2003) 002.

[36] L. Sriramkumar and T. Padmanabhan, Initial state of matter fields and trans-Planckian physics: Can CMB observations disentangle the two?, Phys. Rev. D **71,** 103512 (2005).

[37] G. Nicholson and C. R. Contaldi, The large scale CMB cut-off and the tensor-to-scalar ratio, J. Cosmol. Astropart. Phys. 01 (2008) 002.

[38] L. T. Hergt, W. J. Handley, M. P. Hobson, and A. N. Lasenby, Case for kinetically dominated initial conditions for inflation, Phys. Rev. D **100,** 023502 (2019).

[39] H. V. Ragavendra, D. Chowdhury, and L. Sriramkumar, Suppression of scalar power on large scales and associated bispectra, Phys. Rev. D **106,** 043535 (2022).

[40] D. Wands, Multiple field inflation, Lect. Notes Phys. **738,** 275 (2008).

[41] A. Achucarro, J.-O. Gong, S. Hardeman, G. A. Palma, and S. P. Patil, Features of heavy physics in the CMB power spectrum, J. Cosmol. Astropart. Phys. 01 (2011) 030.

[42] X. Gao, D. Langlois, and S. Mizuno, Oscillatory features in the curvature power spectrum after a sudden turn of the inflationary trajectory, J. Cosmol. Astropart. Phys. 10 (2013) 023.

[43] T. Noumi and M. Yamaguchi, Primordial spectra from sudden turning trajectory, J. Cosmol. Astropart. Phys. 12 (2013) 038.

[44] M. Braglia, D. K. Hazra, L. Sriramkumar, and F. Finelli, Generating primordial features at large scales in two field models of inflation, J. Cosmol. Astropart. Phys. 08 (2020) 025.

[45] G. W. Horndeski, Second-order scalar-tensor field equations in a four-dimensional space, Int. J. Theor. Phys. **10,** 363 (1974).

[46] C. Deffayet, G. Esposito-Farese, and A. Vikman, Covariant Galileon, Phys. Rev. D **79,** 084003 (2009).

[47] C. Deffayet, S. Deser, and G. Esposito-Farese, Generalized Galileons: All scalar models whose curved background extensions maintain second-order field equations and stress-tensors, Phys. Rev. D **80,** 064015 (2009).

[48] T. Kobayashi, M. Yamaguchi, and J. Yokoyama, Generalized G-inflation: Inflation with the most general second-order field equations, Prog. Theor. Phys. **126,** 511 (2011).

[49] S. Karydas, E. Papantonopoulos, and E. N. Saridakis, Successful Higgs inflation from combined nonminimal and derivative couplings, Phys. Rev. D **104,** 023530 (2021).

[50] L. Amendola, Cosmology with nonminimal derivative couplings, Phys. Lett. B **301,** 175 (1993).

[51] G. Tumurtushaa, Inflation with derivative self-interaction and coupling to gravity, Eur. Phys. J. C **79,** 920 (2019).

[52] M. Rinaldi, Black holes with non-minimal derivative coupling, Phys. Rev. D **86,** 084048 (2012).

[53] A. Anabalon, A. Cisterna, and J. Oliva, Asymptotically locally AdS and flat black holes in Horndeski theory, Phys. Rev. D **89,** 084050 (2014).

[54] Y. Ema, R. Jinno, K. Mukaida, and K. Nakayama, Particle production after inflation with non-minimal derivative coupling to gravity, J. Cosmol. Astropart. Phys. 10 (2015) 020.

[55] A. Ghalee, A new phase of scalar field with a kinetic term non-minimally coupled to gravity, Phys. Lett. B **724,** 198 (2013).

[56] C. Fu, P. Wu, and H. Yu, Primordial black holes from inflation with nonminimal derivative coupling, Phys. Rev. D **100,** 063532 (2019).

[57] S. Heydari and K. Karami, Primordial black holes in nonminimal derivative coupling inflation with quartic potential and reheating consideration, Eur. Phys. J. C **82,** 83 (2022).

[58] S. Heydari and K. Karami, Primordial black holes ensued from exponential potential and coupling parameter in nonminimal derivative inflation model, J. Cosmol. Astropart. Phys. 03 (2022) 033.

[59] A. Lewis and S. Bridle, Cosmological parameters from CMB and other data: A Monte Carlo approach, Phys. Rev. D **66,** 103511 (2002).

[60] T. Kobayashi, Horndeski theory and beyond: A review, Rep. Prog. Phys. **82,** 086901 (2019).

[61] I. Quiros, T. Gonzalez, U. Nucamendi, R. García-Salcedo, F. A. Horta-Rangel, and J. Saavedra, On the phantom barrier crossing and the bounds on the speed of sound in non-minimal derivative coupling theories, Classical Quantum Gravity **35,** 075005 (2018).

[62] S. D. H. Hsu, A. Jenkins, and M. B. Wise, Gradient instability for w < −1, Phys. Lett. B **597,** 270 (2004).

[63] B. P. Abbott et al. (LIGO Scientific, Virgo, Fermi-GBM, INTEGRAL Collaborations), Gravitational waves and gamma-rays from a binary neutron star merger: GW170817 and GRB 170817A, Astrophys. J. Lett. **848,** L13 (2017).

[64] Y. Gong, E. Papantonopoulos, and Z. Yi, Constraints on scalar–tensor theory of gravity by the recent observational results on gravitational waves, Eur. Phys. J. C **78,** 738 (2018).

[65] I. Dalianis, S. Karydas, and E. Papantonopoulos, Generalized non-minimal derivative coupling: Application to inflation and primordial black hole production, J. Cosmol. Astropart. Phys. 06 (2020) 040.

[66] M. Braglia, X. Chen, and D. K. Hazra, Primordial standard clock models and CMB residual anomalies, Phys. Rev. D **105,** 103523 (2022).

[67] D. K. Hazra, D. Paoletti, I. Debono, A. Shafieloo, G. F. Smoot, and A. A. Starobinsky, Inflation story: Slow-roll and beyond, J. Cosmol. Astropart. Phys. 12 (2021) 038.

[68] M. Braglia, X. Chen, and D. K. Hazra, Uncovering the history of cosmic inflation from anomalies in cosmic microwave background spectra, Eur. Phys. J. C **82,** 498 (2022).

[69] D. K. Hazra, A. Shafieloo, G. F. Smoot, and A. A. Starobinsky, Inflation with Whip-Shaped Suppressed Scalar Power Spectra, Phys. Rev. Lett. **113,** 071301 (2014).

[70] N. Aghanim et al. (Planck Collaboration), Planck 2018 results. V. CMB power spectra and likelihoods, Astron. Astrophys. **641,** A5 (2020).

[71] A. Lewis, A. Challinor, and A. Lasenby, Efficient computation of CMB anisotropies in closed FRW models, Astrophys. J. **538,** 473 (2000).

[72] M. Powell, The BOBYQA algorithm for bound constrained optimization without derivatives, Technical Report, Department of Applied Mathematics and Theoretical Physics, 2009, https://www.semanticscholar.org/paper/The-BOBYQA-algorithm-for-bound-constrained-without-Powell/0d2edc46f81f9a0b0b62937507ad977b46729f64.

[73] A. Lewis, GetDist: A Python package for analysing Monte Carlo samples, arXiv:1910.13970.

[74] A. Gelman and D. B. Rubin, Inference from iterative simulation using multiple sequences, Stat. Sci. **7,** 457 (1992).

[75] M. Braglia, X. Chen, and D. K. Hazra, Comparing multi-field primordial feature models with the Planck data, J. Cosmol. Astropart. Phys. 06 (2021) 005.

[76] D. K. Hazra, D. Paoletti, M. Ballardini, F. Finelli, A. Shafieloo, G. F. Smoot, and A. A. Starobinsky, Probing features in inflaton potential and reionization history with future CMB space observations, J. Cosmol. Astropart. Phys. 02 (2018) 017.

[77] G. Domènech and M. Kamionkowski, Lensing anomaly and oscillations in the primordial power spectrum, J. Cosmol. Astropart. Phys. 11 (2019) 040.

[78] G. Domènech, X. Chen, M. Kamionkowski, and A. Loeb, Planck residuals anomaly as a fingerprint of alternative scenarios to inflation, J. Cosmol. Astropart. Phys. 10 (2020) 005.

[79] X. Chen, C. Dvorkin, Z. Huang, M. H. Namjoo, and L. Verde, The future of primordial features with large-scale structure surveys, J. Cosmol. Astropart. Phys. 11 (2016) 014.

[80] M. Ballardini, F. Finelli, C. Fedeli, and L. Moscardini, Probing primordial features with future galaxy surveys, J. Cosmol. Astropart. Phys. 10 (2016) 041; 04 (2018) E01.

[81] M. Ballardini, F. Finelli, R. Maartens, and L. Moscardini, Probing primordial features with next-generation photometric and radio surveys, J. Cosmol. Astropart. Phys. 04 (2018) 044.

[82] G. A. Palma, D. Sapone, and S. Sypsas, Constraints on inflation with LSS surveys: Features in the primordial power spectrum, J. Cosmol. Astropart. Phys. 06 (2018) 004.

[83] B. L'Huillier, A. Shafieloo, D. K. Hazra, G. F. Smoot, and A. A. Starobinsky, Probing features in the primordial perturbation spectrum with large-scale structure data, Mon. Not. R. Astron. Soc. **477,** 2503 (2018).

[84] F. Beutler, M. Biagetti, D. Green, A. Slosar, and B. Wallisch, Primordial features from linear to nonlinear scales, Phys. Rev. Res. **1,** 033209 (2019).

[85] M. Ballardini, R. Murgia, M. Baldi, F. Finelli, and M. Viel, Non-linear damping of superimposed primordial oscillations on the matter power spectrum in galaxy surveys, J. Cosmol. Astropart. Phys. 04 (2020) 030.

[86] M. S. Esmaeilian, M. Farhang, and S. Khodabakhshi, Detectable data–driven features in the primordial scalar power spectrum, Astrophys. J. **912,** 104 (2021).

[87] Y. Li, H.-M. Zhu, and B. Li, Nonlinear reconstruction of features in the primordial power spectrum from large-scale structure, Mon. Not. R. Astron. Soc. **514,** 4363 (2022).

[88] M. Ballardini, F. Finelli, F. Marulli, L. Moscardini, and A. Veropalumbo, New constraints on primordial features from the galaxy two-point correlation function, Phys. Rev. D **107,** 043532 (2023).

[89] I. Debono, D. K. Hazra, A. Shafieloo, G. F. Smoot, and A. A. Starobinsky, Constraints on features in the inflationary potential from future Euclid data, Mon. Not. R. Astron. Soc. **496,** 3448 (2020).

[90] D. Chandra and S. Pal, Investigating the constraints on primordial features with future cosmic microwave background and galaxy surveys, J. Cosmol. Astropart. Phys. 09 (2022) 024.

[91] X. Chen, P. D. Meerburg, and M. Münchmeyer, The future of primordial features with 21 cm tomography, J. Cosmol. Astropart. Phys. 09 (2016) 023.

[92] Y. Xu, J. Hamann, and X. Chen, Precise measurements of inflationary features with 21 cm observations, Phys. Rev. D **94,** 123518 (2016).

[93] S. Balaji, H. V. Ragavendra, S. K. Sethi, J. Silk, and L. Sriramkumar, Observing Nulling of Primordial Correlations via the 21 cm Signal, Phys. Rev. Lett. **129,** 261301 (2022).

[94] A. Kogut et al., The primordial inflation explorer (PIXIE): A nulling polarimeter for cosmic microwave background observations, J. Cosmol. Astropart. Phys. 07 (2011) 025.

[95] P. André et al. (PRISM Collaboration), PRISM (Polarized radiation imaging and spectroscopy mission): An extended white paper, J. Cosmol. Astropart. Phys. 02 (2014) 006.

[96] S. Chabanier, M. Millea, and N. Palanque-Delabrouille, Matter power spectrum: From Lyα forest to CMB scales, Mon. Not. R. Astron. Soc. **489,** 2247 (2019).

[97] X. Chen, R. Easther, and E. A. Lim, Large non-Gaussianities in single field inflation, J. Cosmol. Astropart. Phys. 06 (2007) 023.

[98] X. Chen, R. Easther, and E. A. Lim, Generation and characterization of large non-Gaussianities in single field inflation, J. Cosmol. Astropart. Phys. 04 (2008) 010.

[99] P. Adshead, C. Dvorkin, W. Hu, and E. A. Lim, Non-Gaussianity from step features in the inflationary potential, Phys. Rev. D **85,** 023531 (2012).

[100] D. K. Hazra, L. Sriramkumar, and J. Martin, BINGO: A code for the efficient computation of the scalar bi-spectrum, J. Cosmol. Astropart. Phys. 05 (2013) 026.

[101] J. R. Fergusson, H. F. Gruetjen, E. P. S. Shellard, and M. Liguori, Combining power spectrum and bispectrum measurements to detect oscillatory features, Phys. Rev. D **91,** 023502 (2015).

[102] J. R. Fergusson, H. F. Gruetjen, E. P. S. Shellard, and B. Wallisch, Polyspectra searches for sharp oscillatory features in cosmic microwave sky data, Phys. Rev. D **91,** 123506 (2015).

[103] K. N. Abazajian et al. (CMB-S4 Collaboration), CMB-S4 Science Book, First Edition, arXiv:1610.02743.

[104] M. Hazumi et al. (LiteBIRD Collaboration), LiteBIRD: JAXA's new strategic L-class mission for all-sky surveys of cosmic microwave background polarization, Proc. SPIE Int. Soc. Opt. Eng. **11443,** 114432F (2020).

[105] A. Lee et al., LiteBIRD: An all-sky cosmic microwave background probe of inflation, Bull. Am. Astron. Soc. **51,** 286 (2019).

[106] P. Ade et al. (Simons Observatory Collaboration), The Simons Observatory: Science goals and forecasts, J. Cosmol. Astropart. Phys. 02 (2019) 056.

[107] M. H. Abitbol et al. (Simons Observatory Collaboration), The Simons Observatory: Astro2020 Decadal Project Whitepaper, Bull. Am. Astron. Soc. **51,** 147 (2019).

[108] CMB-Bharat, http://cmb-bharat.in.